

**EXPERIMENTAL INVESTIGATION OF A STRATIFIED**

**BUOYANT WAKE**

A Thesis

by

WAYNE N. KRAFT

Submitted to the Office of Graduate Studies of  
Texas A&M University  
in partial fulfillment of the requirements for the degree of

MASTER OF SCIENCE

August 2004

Major Subject: Mechanical Engineering

**EXPERIMENTAL INVESTIGATION OF A STRATIFIED**

**BUOYANT WAKE**

A Thesis

by

WAYNE N. KRAFT

Submitted to Texas A&M University  
in partial fulfillment of the requirements  
for the degree of

MASTER OF SCIENCE

Approved as to style and content by:

---

Malcolm Andrews  
(Chair of Committee)

---

Gerald Morrison  
(Member)

---

Paul Cizmas  
(Member)

---

Dennis O'Neal  
(Head of Department)

August 2004

Major Subject: Mechanical Engineering

**ABSTRACT**

Experimental Investigation of a Stratified Buoyant Wake.

(August 2004)

Wayne N. Kraft, B.S., Texas A&M University

Chair of Advisory Committee: Dr. Malcolm Andrews

An existing water channel facility at Texas A&M University is used to experimentally study a stratified, buoyant wake. A cylindrical obstruction placed at the centerline of a developing Rayleigh-Taylor mixing layer serves to disturb the equilibrium of the Rayleigh-Taylor mixing layer. The development of the near wake in the presence of unstable stratification is examined, in addition to the recovery of the buoyancy driven mixing layer. Planar laser induced fluorescence (PLIF) is used to visualize the mixing layer / wake interactions, and qualitative observations of the behavior have been made. Also, quantitative measurements of velocity fluctuations and density fluctuations in the near wake have been obtained using particle image velocimetry (PIV) and a high resolution thermocouple system. These experimental measurements were used to investigate how the wake and buoyancy driven mixing layer interact. Finally, a mathematical model has been used to describe the decay of vertical velocity fluctuations in the near wake due to the effects of buoyancy.

## ACKNOWLEDGEMENTS

I would like to thank my research advisor, Malcolm J. Andrews, for his help in completing this work. I would also like to thank my co-workers, especially Nicholas Mueschke and Praveen Ramaprabhu, for their help. Finally I would like to thank my friends and family for their support and repeated inquiries concerning when I was graduating, which helped to motivate me as I neared the completion of this work.

This research has been funded by the U.S. Department of Energy from DOE Grant # DE-FG03-99DP00276/A000.

## TABLE OF CONTENTS

	Page
ABSTRACT .....	iii
ACKNOWLEDGEMENTS .....	iv
TABLE OF CONTENTS .....	v
LIST OF FIGURES.....	vii
LIST OF TABLES.....	ix
1. INTRODUCTION.....	1
1.1 Preliminaries - significance.....	1
1.2 The buoyant wake .....	2
1.3 Literature survey .....	4
1.3.1 Buoyancy effects in wakes.....	5
1.3.2 An overview of Rayleigh-Taylor ( buoyancy) driven turbulence.....	7
1.4 Objectives.....	9
1.5 Overview of research .....	10
2. EXPERIMENTAL SETUP AND DIAGNOSTICS.....	11
2.1 Description of experiment.....	11
2.2 Diagnostics.....	13
2.2.1 Particle image velocimetry (PIV).....	14
2.2.2 Thermocouple system.....	15
2.2.3 Planar laser induced fluorescence (PLIF) .....	16
3. VERIFICATION OF THE EXPERIMENTAL SETUP .....	19
4. OBSERVATIONS.....	24
5. EXPERIMENTAL DATA AND ANALYSIS .....	33
5.1 Vertical velocity fluctuations in the near wake .....	33

	Page
5.2 Molecular mixing in the near wake.....	39
5.3 Recovery of the buoyancy-driven turbulence .....	43
6. A MATHEMATICAL MODEL FOR DECAYING VELOCITY FLUCTUATIONS IN THE NEAR FIELD OF A BUOYANT WAKE .....	47
7. CONCLUSIONS .....	60
REFERENCES .....	65
APPENDIX A .....	69
APPENDIX B .....	72
VITA.....	77

## LIST OF FIGURES

FIGURE	Page
1. Schematic of the experimental apparatus.....	11
2. Flow channel test section with cylindrical obstruction. ....	12
3. Visualization of the wake behind a cylinder with no buoyancy for a cylinder diameter of 1.6 cm and free stream velocity of 4 cm/s.....	19
4. Instantaneous vector field and vorticity contours for the near wake of a cylinder with no buoyancy. ....	20
5. Comparison of streamwise peak values $u'_{rms}$ of the current experiment with experimental data from other researchers for a wake from a cylinder. ....	21
6. Comparison of cross stream peak values $v'_{rms}$ of the current experiment with experimental data from other researchers for a wake from a cylinder.....	22
7. Visualizations of the buoyancy driven wake using Nigrosene dye. (A) Buoyancy driven mixing layer (B) Buoyancy driven mixing layer and wake with a cylinder of $D = 1.6$ cm (C) Buoyancy driven mixing layer and wake with a cylinder of $D=3.25$ cm. $U = 4$ cm/s for all three experiments. ....	25
8. PLIF images in the near field of an unstably stratified wake.....	29
9. Visualizations of buoyancy effects on wakes using Nigrosene dye. (A) Buoyant wake (B) Wake with stabilizing buoyancy (C) Wake without buoyancy effects. All three wakes are formed from flow around a cylinder of $D = 1.6$ cm and $U = 4$ cm/s. ....	31
10. Decay of vertical velocity fluctuations, $v'_{rms}$ , in the wake of a cylinder with stable buoyancy (triangles), unstable buoyancy (squares), no buoyancy (circles), and a typical Rayleigh Taylor mixing layer for the same experimental conditions (dashed line).....	34

FIGURE	Page
11. Decay of vertical velocity fluctuations, $v'_{rms}$ , in the very near wake of a cylinder with stable buoyancy, unstable buoyancy, and no buoyancy. ....	36
12. Variation of the location of peak $v'_{rms}$ with mixing layer turbulence level. Flow conditions for both cases were with a $U = 4.4$ cm/s, $A = 5 \times 10^{-4}$ and $D = 1.6$ cm. ....	37
13. Evolution of the molecular mix parameter, $\theta$ , in the near wake. Measured from centerline density fluctuations. Data for the Rayleigh Taylor mixing layer obtained from Ramaprabhu and Andrews (2004). ....	40
14. A comparison of power spectra of centerline density fluctuations in the buoyant wake (solid black line) and a mixing layer driven by the Rayleigh-Taylor instability (dotted red line) obtained from Ramaprabhu (2003). ....	42
15. Demonstration of the recovery of buoyancy driven turbulence through the determination of $\alpha$ from $v' / 2Agt$ . ....	44
16. Power spectra of centerline $v'$ in the buoyant wake for a cylinder diameter of 1.6 cm and $A = 5 \times 10^{-4}$ . ....	45
17. Decay of $v'_{rms}$ in the near wake for the cases of no buoyancy, stable buoyancy, and unstable buoyancy as determined from the model solutions using $C_D = 0.42$ and for $A = \pm 5 \times 10^{-4}$ . ....	54
18. $1/(a_0 t + a_1)$ decay of vertical velocity fluctuations in the near wake for a cylinder wake without buoyancy. ....	55
19. Recovery of buoyancy driven turbulence as demonstrated by the model solution for $D = 1.6$ cm, $U = 4$ cm, and $A = 5 \times 10^{-4}$ with $C_D = 0.59$ . ....	58



**LIST OF TABLES**

TABLE	Page
1. Experimental parameters.....	13
2. Summary of decay rates of vertical velocity fluctuations.....	38
3. Comparison of $v'$ decay rates for the transport model and experimental results using a $C_D = 0.42$ .....	55
4. Comparison of $C_D$ for the mathematical model. ....	56

## 1. INTRODUCTION

### *1.1 Preliminaries - significance*

Exploration of turbulent wakes in a buoyant environment offers a unique opportunity to study the chaotic nature of turbulence. This investigation focuses on the dynamics of a buoyant wake. The wake is generated by turbulent flow moving past a cylindrical obstruction. Turbulence upstream of the cylinder, driven by the Rayleigh-Taylor instability, interacts with the wake. The resulting development of the near wake and subsequent recovery of the buoyancy dominated turbulence is examined.

Engineers and scientists have endeavored to understand the dynamics of wakes. The periodic nature and organized structure of a wake are often observed in environments otherwise dominated by disorder. In nature, wakes can be seen at small scales as water moves around obstructions in rivers, or at large scales as vortex trails form in the atmosphere as bodies of air move around land masses (Berger and Willie 1972). The effects of buoyancy on naturally formed wakes can be observed in ocean currents, or as air moves over mountains into heavy, pollution surrounding cities (Lin and Pao 1979). Ultimately an understanding of wake flow satisfies both academic interests in fluid flows and turbulence, and for the development of improvements in technology for industrial applications. As a result, much effort has been given to

---

This thesis follows the style of the *Journal of Fluid Mechanics*.

understanding the organization, structure, and development of wakes in general. The inclusion of buoyancy effects in the dynamics of wake has been recently studied, as it offers insight into the role of buoyancy in the production of turbulence.

The motivation of this research is to provide insight into the non-equilibrium development of turbulent mixing which occurs in Inertial Confinement Fusion (ICF). ICF relies on the implosion of target capsules to produce thermonuclear reactions. Hydrodynamic instability has an important role in the implosion phase of inertial confinement fusion, as buoyancy driven mixing limits the energy yield of the overall process (Lindl 1998). During ICF, shockwaves pass through the turbulent mix, depositing momentum and disturbing the equilibrium growth of the buoyancy driven mixing. The interaction of the Rayleigh-Taylor instability and the passing shockwave is not well understood. Although the specific dynamics occurring in the ICF process cannot be replicated in the current experiment, the very similar interaction of the Rayleigh-Taylor instability with a disturbance of its equilibrium can be examined.

### *1.2 The buoyant wake*

Buoyancy driven turbulence occurs in an unstably stratified flow with a heavy fluid above a light fluid. With unstable stratification, if the pressure and density are constant in every horizontal plane, the stratification is in unstable equilibrium (Turner 1973). In particular, the Rayleigh-Taylor fluid instability arises when a pressure gradient is imposed on a density gradient along the interface of two fluids (Chandrasekhar 1961) with  $\nabla p \bullet \nabla \rho < 0$ . The buoyancy driven growth of perturbations proceed through linear

instability, nonlinear instability, and finally forming a turbulent mix which grows in a self-similar nature (Youngs 1984). The governing parameter of the buoyancy driven instability is the Atwood number,  $A = (\rho_1 - \rho_2)/(\rho_1 + \rho_2)$ , where  $\rho_1$  and  $\rho_2$  are the heavy and light fluid densities, respectively.

When a wake is introduced to the buoyancy driven mix, it disturbs the equilibrium of the Rayleigh-Taylor mixing region. Shear layers shed from the cylinder surface roll-up into vortices in a periodic manner behind the cylinder, and viscous effects dissipate the subsequent turbulent motion. Buoyancy (through associated potential energy) however serves as a source of turbulent kinetic energy inside the wake. Potential energy, stored in the mean flow through unstable density gradients, is converted to turbulent kinetic energy as the fluids overturn. Eventually downstream from the cylinder, a balance is found between the dissipation of the wake and turbulent energy production from buoyancy. The buoyancy driven turbulence recovers from the disturbance of the cylinder and the Rayleigh-Taylor mixing layer returns to its equilibrium growth.

A Reynolds number for the wake is usually defined as  $Re = UD/\nu$  (Williamson 1996). Above a critical Reynolds number,  $140 \leq Re \leq 190$ , the wake becomes turbulent (Williamson 1996). The results to be presented are in a  $Re$  range of  $640 \leq Re \leq 690$ , and thus above the critical Reynolds number. Effects of stratification in the wake are included in the characteristic buoyancy frequency, where  $N^2 = -g/\rho_0 (\partial\rho/\partial z)$ . The evaluation of  $N$  requires knowledge of the density gradient,  $\partial\rho/\partial z$ , which may be approximated as  $(\rho_1 - \rho_2)/D$  for the turbulent mixing layer around the cylinder. It is also

useful to determine the ratio of inertial forces to buoyancy forces, given by the internal Froude number,  $Fi = U/ND$ . This non-dimensional parameter is a function of the free stream velocity, characteristic buoyancy frequency, and diameter of the cylinder. As  $Fi \rightarrow 0$  the effects of stratification become more dominant. The internal Froude number has been utilized extensively in describing the stably stratified wake (Spedding 1997 and Xu *et al.* 1995), however it cannot accurately describe the physical nature of the current work. The characteristic buoyancy frequency utilized in  $Fi$ , arises from the internal waves generated by the restoring force of stabilizing buoyancy (light fluid above heavy). For unstable stratification (heavy fluid above light) and associated buoyancy driven turbulence, the internal waves do not appear and therefore  $Fi$  is not directly relevant. However, it is useful to calculate  $Fi$  to illustrate the difference in flow regimes between the current work and previous research in stratified wakes. The magnitude of  $Fi$  provides a direct comparison between the ratio of inertial forces to buoyancy forces in stably stratified wakes. The negative value of  $\partial\rho/\partial z$  for unstably stratified flow, requires the use of  $Fi^2$  for a meaningful comparison to be made. Therefore, flows with unstable density gradients result in a negative value of  $Fi^2$  whereas flow with a stable density gradient has a positive value for  $Fi^2$ .

### *1.3 Literature survey*

A literature survey of related work in stratified wakes and buoyancy driven turbulence is described next. An overview of the current state of research of stratified wakes will be shown, illustrating the uniqueness of the current research. In addition,

previous experiments in buoyancy driven turbulence, including those conducted on the current experimental apparatus, will be described.

### *1.3.1 Buoyancy effects in wakes*

Early investigations of wakes focused primarily on the near wake structure, excluding buoyancy effects, as illustrated in a comprehensive review by Williamson (1996). Only more recently have researchers sought to understand the effects of buoyancy in the turbulent wake. In general this has been limited to the inclusion of stabilizing buoyancy (light fluid above heavy). The earliest investigations of stratified wakes were performed by Pao (1973). A stratified, turbulent wake was created by towing a cylinder or grid through a tank with stably stratified salt water. Pao reported spectra of turbulent velocity and density measurements in the wake region.

Recent experiments in stratified wakes were performed by Xu *et al.* (1995), Spedding (1997, 2002), and Bonnier & Eiff (2002). Spedding (1997, 2002) and Bonnier & Eiff (2002) describe the structure and decay of a turbulent axisymmetric wake subjected to stabilizing buoyancy. The behavior and kinetic energy decay rate of the near wake with large Froude number flows were found to be unaffected by the presence of stable stratification. However at an intermediate stage of development, however, the effect of stabilizing buoyancy is evident. In this intermediate stage, buoyancy forces arising from the stable stratification overcome the available kinetic energy. The turbulent kinetic energy is no longer sufficient to increase the average turbulent eddy size. At the same time, fluid displaced from its equilibrium position by the wake

instability relaxes back to its equilibrium position. The relaxing process converts potential energy to kinetic energy, decreasing the kinetic energy decay rate. In the final stage of wake development, fine scale turbulence motions are damped out and only the large scale structure from the vortex shedding are present. Re-stratification of the wake and the relaxing process of displaced fluid completes, resulting in an increase of the kinetic energy decay rate. A similar analysis was performed by Xu *et al.* (1995), investigating the turbulent wake behind a cylinder in a stably stratified flow. At high Re, the stratified plane wake could be divided into regimes based on Froude number alone. Stratified turbulence models were compared with the stratified wake to provide insight into stably stratified, turbulent flows. The common theme of these researchers is the study of *stabilizing* buoyancy in the study of near wake behavior.

Studies of unstable, buoyant wakes however are few. Mixed convection from flow around a heated cylinder was experimentally studied by Oosthuizen and Madan (1971). However, this was a convection heat transfer study, and did not involve an analysis of the wake dynamics. A numerical study of the near wake dynamics behind a heated/cooled cylinder was performed by Chang and Sa (1990). Chang and Sa observed a weakened roll-up of vortices in the near wake and an increase in vortex shedding frequency with increased heating of the cylinder. These studies were all that were found regarding the effect of unstably buoyancy on wakes. The present investigation is seemingly unique, and examines the effect of unstable buoyancy on the development and behavior of the near wake

### *1.3.2 An overview of Rayleigh-Taylor (buoyancy) driven turbulence*

As previously stated, buoyancy-driven turbulence occurs in a unstably stratified flow when a heavy fluid rests above a light fluid. Small perturbations at the interface of the two fluids grow as a result of the Rayleigh-Taylor instability, developing eventually into a turbulent mixing layer. Potential energy from the heavy fluid supplies energy for the turbulent motions as it falls through the lighter fluid. The difficulty of studying this phenomena is creating and controlling the unstable density gradient and interface between the two fluids. As a result, many creative approaches have been used to study buoyancy driven turbulence and the Rayleigh-Taylor instability. The experiments of Read (1984) accelerated a tank containing light and heavy fluids initially at rest. The tank was accelerated downward using rocket motors at a rate of 25 – 75 times gravity. However, the acceleration of the tank was not constant and data collection times were severely limited by the high accelerations. A similar method of examining the Rayleigh-Taylor instability was performed by Dimonte & Schneider (1996), where, instead of rocket motors a linear electric motor (LEM) was used to accelerate the tank downward. The LEM gave a constant acceleration of the tank, but again resulted in short data collection times. Measurements by both Read (1984) and Dimonte & Schneider (1996) were capable of demonstrating a quadratic growth of the mixing layer half width,  $h$ , once memory of the initial conditions were lost. This is in agreement with the dimensional analysis of Youngs (1984), where  $h$  is a function of the Atwood number ( $A$ ), the gravitational acceleration ( $g$ ), time ( $t$ ), and the growth constant ( $\alpha$ , with a measured range of 0.05 to 0.1).



$$h = \alpha A g t^2 \quad (1)$$

As an alternative to the described experimental methods, a water channel facility at Texas A&M has been used extensively to study buoyancy-driven turbulence. The water channel is used to study the turbulent mixing layer and the Rayleigh-Taylor instability in the same manner as shear mixing layers were studied by Lawrence and Browand (1991). The advantage of such an experimental setup is the long data collection times and the statistically steady nature of the experiment. Early work using the water channel facility was performed by Snider and Andrews (1994). Snider was able to validate the experimental setup and uniquely present statistical measurements inside a buoyancy driven mixing layer. Snider's measurements included the growth rate and turbulent mixing for the developing Rayleigh-Taylor instability. In addition, Snider examined the combined effects of buoyancy and shear in a mixing layer. The work of Snider was later expanded by Wilson and Andrews (2002). In addition to studying the combined effects of buoyancy and shear in turbulence, Wilson made spectral measurements of density fluctuations inside the mixing layer to better understand the mixing process. Particle image velocimetry (PIV) was also utilized to obtain velocity spectra inside the mixing layer. The work of Snider and Andrews (1994) and Wilson and Andrews (2002) provided observations of the overall behavior and development of a buoyancy-driven mixing layer. A more detailed description of the self-similar behavior of the mixing layer was performed by Ramaprabhu and Andrews (2004), using PIV and a high resolution thermocouple system. Spectral measurements of both velocity and density were used to characterize the self similar nature of buoyancy driven turbulence.

The investigations performed by previous researchers utilizing the water channel facility described the equilibrium growth of the Rayleigh-Taylor instability. The current research aims to disturb the equilibrium growth of the buoyancy driven mixing layer using an obstruction. Utilizing many of the measurement techniques developed by previous researchers using the water channel facility and with the introduction of PLIF by the present researcher, development of the near wake with unstable stratification and the recovery of the buoyancy driven turbulence is examined.

#### *1.4 Objectives*

The objectives of the present research are to:

- Disturb a Rayleigh-Taylor mixing layer using a cylindrical obstruction.
- Measure the response of the subsequent wake to unstable stratification.
- Measure the recovery of the mixing layer from a disturbance of its equilibrium.
- Understand the mechanisms for recovery to equilibrium growth of the Rayleigh-Taylor instability.
- Develop a mathematical model to describe the effects of buoyancy on the near wake behavior.

These objectives are accomplished through an experimental investigation utilizing the existing water channel facility at Texas A&M University. The water channel facility has been modified to include an obstruction to disturb the mixing layer. Particle image velocimetry (PIV), a high-resolution thermocouple system, and planar

laser induced fluorescence (PLIF) are used to measure the response of the plane wake to buoyancy driven turbulence. Qualitative observations from visualizations of the wake / mixing layer interactions are also made. In addition, quantitative results of fluctuating velocity components, density measurements, and velocity fluctuation decay rates are measured for a wake under the influence of no buoyancy, stabilizing buoyancy, and unstable buoyancy. A simple model of the near wake behavior of the velocity fluctuations will also be proposed to describe the competing dynamics in the wake.

### *1.5 Overview of research*

A turbulent mixing layer driven by the Rayleigh-Taylor instability is disturbed by a cylindrical obstruction and the interactions of the competing equilibria are experimentally studied. Included in the subsequent discussion is a presentation of the experimental setup and measurement techniques. In addition, qualitative observations from visualizations of the wake / mixing layer interactions are presented. Quantitative results of fluctuating velocity components, density measurements, and velocity fluctuation decay rates are presented for a wake under the influence of no buoyancy, stabilizing buoyancy, and unstable buoyancy. A mathematical model of the near wake behavior of the velocity fluctuations is included to describe the competing dynamics in the wake and the effects of buoyancy. Finally, conclusions from this experimental investigation are discussed.

## 2. EXPERIMENTAL SETUP AND DIAGNOSTICS

### 2.1 Description of experiment

The experimental apparatus consists of a Plexiglas flow channel with an inlet and exit plenum. A schematic of the experimental apparatus is shown in Figure 1. The flow channel is 100 cm in length, 32 cm deep, and has a width of 20 cm. Water is supplied to the flow channel via the inlet plenum from two 500 gallon supply tanks. Two parallel streams of water enter the inlet plenum and are separated by a splitter plate. Prior to the test section, a series of flow straighteners and wire meshes are utilized

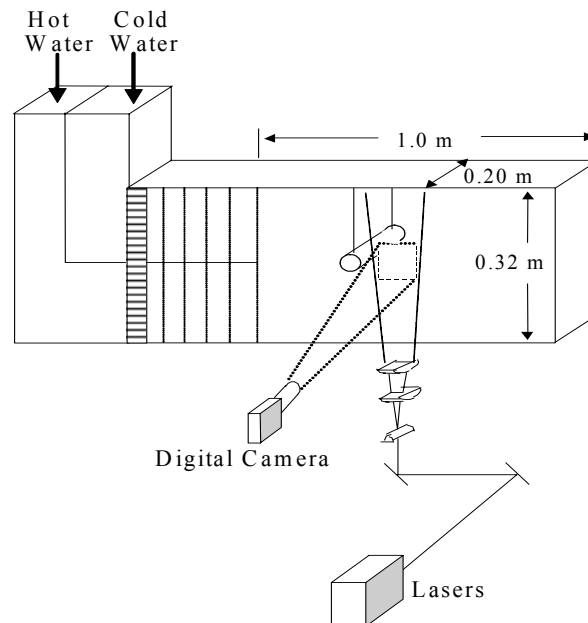


Figure 1. Schematic of the experimental apparatus.

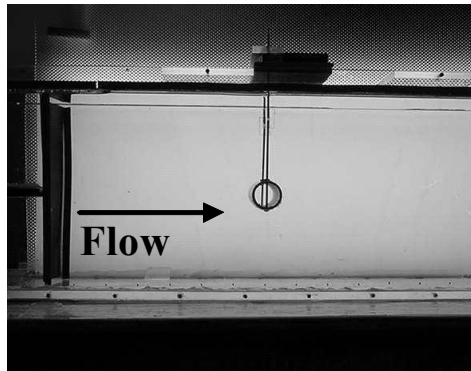


Figure 2. Flow channel test section with cylindrical obstruction.

to minimize the free stream turbulence (Snider and Andrews 1994). The splitter plate is 0.32 cm thick and the end has a knife-edge with an included angle of  $2.5^\circ$ . At the end of the splitter plate the two streams are allowed to mix. To reduce the momentum deficit created by the knife-edge, a fine wire mesh is placed at the end of the splitter plate. The mean flow rate is adjusted using calibrated rotameters. Desired stratification in the test section is achieved by adjusting the temperatures of the two supply tanks. A uniform temperature in each supply tank is ensured using sump pumps to completely mix each water supply. For unstable stratification, cold (heavy) water enters the test section above hot (light) water. Temperature differences between the two inlet streams range from  $5^\circ\text{C}$  to  $7^\circ\text{C}$ .

In the presence of a small perturbation and unstable stratification, a buoyancy driven mixing layer develops downstream of the splitter plate. The cylinder is aligned with the splitter plate, and thus disrupts the buoyancy driven turbulence. Figure 2 shows the flow channel test section with the cylindrical obstruction. The cylinder is located 30

cm downstream of the splitter plate at the centerline of the mixing layer and is oriented horizontally and perpendicular to the stream wise direction. It is constructed from a section of hollow PVC pipe that is suspended from the top of the flow channel. Table 1 lists the parameter range for experiments of the wake with unstably buoyancy performed using this apparatus.

Mean velocity	$U$ (cm/s)	4.0 - 4.3
Cylinder diameter	$D$ (cm)	1.6
Kinematic viscosity	$\nu$ (cm <sup>2</sup> /s)	0.01
Reynolds number	$Re$	640-690
Internal Froude number	$Fi^2$	-7
Atwood number	$A$	$5 \times 10^{-4}$

Table 1. Experimental parameters.

## 2.2 Diagnostics

The dynamics of the buoyant wake are described through velocity and density measurements at the centerline of the wake. These measurements were taken using particle image velocimetry (PIV), a high-resolution thermocouple system, and planar laser induced fluorescence (PLIF). In addition qualitative observations are made through visualization techniques.

### 2.2.1 Particle image velocimetry (PIV)

PIV is used to obtain velocity measurements in the wake of the cylinder. The PIV system consists of two 120 mJ Nd-YAG pulse lasers, that each fire at a rate of 15 Hz. By alternating the pulse of each laser an effective sampling rate of 30 Hz is achieved. Hollow, silvered glass spheres, approximately 10  $\mu\text{m}$  in diameter, are seeded in each stream at a concentration of 5 – 7.5 ml per 500 gallons of water. A series of cylindrical lenses form a laser sheet of approximately 1 mm thickness, which projects through the water channel vertically. Images of seed particles are captured using a KODAK Megaplug digital camera. Triggering of the camera and lasers are synchronized using a pulse generator. A triggering signal of 30 Hz is output by the digital camera which is divided by the pulse generator into two 15 Hz signals 180° out of phase with respect to each other. These two 15 Hz signals are then used to trigger the flash lamp of the respective lasers. Details of the setup and operation of the triggering system are included in Appendix A. The physical window size captured by the digital camera is 6 cm x 4.5 cm. A *labview* based data acquisition system records 1200 digital images at 640 x 480 pixels. Post processing of the digital images is performed using the MATPIV program. MATPIV utilizes a cross-correlation technique to obtain a velocity field from any two successive images (Grue *et al* 2000). Particle displacements between two images,  $\text{Im}_1$  and  $\text{Im}_2$ , are found from a cross correlation function,  $R(x,y)$ , as

$$R(x, y) = \sum_{i=-M/2, j=-N/2}^{M/2} \text{Im}_1(i, j) \text{Im}_2(i + x, j + y). \quad (2)$$

The distance from the correlation peak to the center of the interrogation window is the displacement vector for a given interrogation window. Vectors lying outside two

standard deviations of neighboring vectors are replaced utilizing an interpolation routine. Multiple passes of the cross-correlation technique are used, starting with an initial interrogation window size of 64 x 64 pixels. Displacement vectors determined from the first pass are used as estimates for a second pass with a smaller interrogation window size of 32 x 32 pixels. In addition each interrogation window has a 50% overlap with its neighbor, which results in a final vector field of 39 x 29 vectors. Using this technique 1199 vector fields are obtained to compute velocity statistics in the wake of the cylinder. The uncertainty in the velocity measurements has been found using techniques described by Adrian (1997) to be 0.05 cm/s (Ramapabraham 2003).

### *2.2.2 Thermocouple system*

Density measurements are performed by using a high-resolution thermocouple system. An E-type thermocouple with a probe diameter of approximately 0.18 mm is suspended in the flow using a vertical rake. The thermocouple is sampled at 50,000 Hz using a 16-bit data acquisition board. To reduce noise, a local average of 100 samples is used to obtain an effective sampling rate of 500 Hz. Measurements are taken for a length of ~ 120 seconds. The accuracy of the thermocouple system is  $\pm 0.1^\circ\text{C}$  (Wilson 2003) and the transient response time for the E-type thermocouple is 0.001 s/ $^\circ\text{C}$  (Wilson and Andrews 2002). Temperature measurements at the centerline of the mixing layer are converted to densities using an equation of state found in Kukulka (1981) as



$$\rho = \frac{999.8396 + 18.2249T - 0.007922T^2 - 55.448 \times 10^{-6} T^3 + 149.756 \times 10^{-9} T^4 - 393.295 \times 10^{-12} T^5}{1 + 18.159 \times 10^{-3} T} \quad (3)$$

The centerline of the mixing layer was determined by traversing the thermocouple through the mixing layer. A displacement coefficient,  $\phi$ , is used to determine the location of the centerline of the mixing layer, where  $\phi = 0.5$  at the centerline. The displacement coefficient,  $\phi = (T_2 - T_{avg}) / (T_2 - T_1)$ , is defined in terms of the cold water stream temperature,  $T_1$ , and hot water stream temperature,  $T_2$ . A detailed description of the thermocouple system can be found in Wilson and Andrews (2002).

### 2.2.3 Planar laser induced fluorescence (PLIF)

Planar laser induced fluorescence (PLIF) is a well documented technique relying on the fluorescent properties of dye markers to create useful visualizations and quantitative data. An advantage of the technique is the ability to make field measurements of a scalar quantity through non-intrusive means. PLIF is capable of both high speed and high resolution measurements without disrupting the fluid flow. By measuring the fluorescence intensity of a dye marker in the fluid flow, related scalar measurements such as concentration or temperature can be determined for the field of view of the image capturing device.

This technique has been used extensively by researchers studying combustion, reactive flows, and turbulent jets across many fields of engineering, with one of the earliest applications performed by Walker (1987). The advantages of PLIF as a visualization tool and the possible measurement of scalar quantities, particularly

concentration, create opportunities for advancement of research in buoyancy driven mixing as well. The application of PLIF to buoyancy driven mixing research and specifically the study of the Rayleigh-Taylor instability has been proven beneficial by Waddell, Niederhaus and Jacobs (2001) through recent experiments and has generated interest in the buoyancy driven mixing research conducted here at Texas A&M (Ramaprabhu and Andrews 2004). Interaction of the plane wake and the buoyancy driven mixing layer is visualized through the use of PLIF.

A dye marker, Rhodamine 6G, is seeded into the cold fluid (top stream) which is excited by the Nd-YAG laser, causing the dye to fluoresce. The emission of a longer wavelength of light by the dye marker allows for a separation of the fluorescent light signal and laser excitation signal with the use of a filter, and is the fundamental mechanism of the PLIF technique. A filter mounted on the CCD camera allows only the fluorescent light signal to be captured.

Rhodamine 6G was chosen for its solubility in water and its fluorescent behavior when excited by the 532 nm wavelength light source of the Nd-YAG lasers. Various concentrations of the dye marker were tried with the range of laser intensities available using the Nd-YAG laser system. A concentration of 2.5 grams / 500 gallons was found suitable for the given experimental setup. Rhodamine 6G is mixed prior to the experiment in the cold water supply tank. The excitation of the dye is accomplished by forming a laser sheet in the water channel at the desired field of view. The laser sheet is created in the same manner as previously described for PIV. Also the method of image capture and synchronization of the lasers and the CCD camera are the same as

previously described. Accurate focusing of the CCD camera is performed before running of the experiment by injecting small amounts of Rhodamine 6G into the laser sheet. The structures created by injecting the dye into the water filled channel are used to focus the camera and determine the approximate camera aperture setting and laser intensity.

The PLIF technique described is only currently used to obtain visualizations of the complex dynamics in buoyancy driven mixing. However there is interest in utilizing the technique to obtain concentration field measurements which can be determined from the fluorescent light intensity. The procedure and analysis to accomplish this however is more intensive, as there are several factors to consider when relating the fluorescent intensity to the dye concentration, including the photochemical process, optical arrangement, and characteristics of the imaging sensor (Karasso and Mungal 1997).

### 3. VERIFICATION OF THE EXPERIMENTAL SETUP

Verification of the experimental setup was performed by analyzing the canonical case of the near wake behind a cylinder with no buoyancy. The results to be presented are obtained at a free stream velocity of 4 cm/s with a cylinder diameter of 1.6 cm. This corresponds to a  $Re = 640$ , above the critical limit for the formation of a periodic, turbulent wake (Williamson 1996). A visualization of the wake is shown in Figure 3 using Nigrosene dye to mark the top water stream. The periodic nature of the wake is clearly visible as the stems of the vortex pairs are present at regular intervals. The turbulent nature of the shedding vortices however results in the three dimensional behavior particularly seen as the wake develops further downstream. The approximate shedding frequency can be determined from the image in Figure 3. By determining the location of the stems of the vortex pairs, an average wavelength for the shedding



Figure 3. Visualization of the wake behind a cylinder with no buoyancy for a cylinder diameter of 1.6 cm and free steam velocity of 4 cm/s.

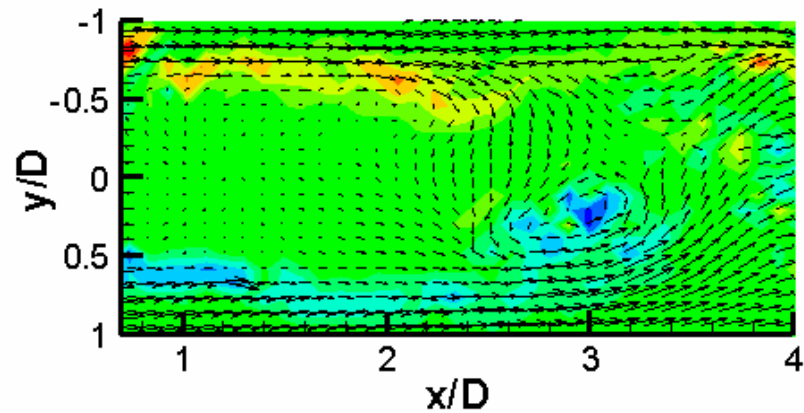


Figure 4. Instantaneous vector field and vorticity contours for the near wake of a cylinder with no buoyancy.

structures is found to be 8.1 cm. Combining this with the free stream velocity of 4.0 cm/s, the shedding frequency from the cylinder is 0.49 Hz. This agrees with the expected shedding frequency of 0.5 Hz, as determined using the Strouhal number, where  $St = 0.2 = fD / U$  ( $f$  is the shedding frequency from the cylinder,  $D$  is the cylinder diameter, and  $U$  is the free stream velocity).

A PIV measured instantaneous vector field with 2-D vorticity contours for the near wake behind the cylinder is shown in Figure 4. Shear layers shed from the top and bottom surfaces of the cylinder are clearly marked by vorticity contours. Roll-up of a shear layer shed from the bottom of the cylinder is evident from the vector field and vorticity contours at approximately  $x/D = 3$ .

To verify the experimental methods used in this experiment, measurements of the peak values of  $u'_{rms}$  and  $v'_{rms}$  obtained using PIV are compared with other experiments for the plane wake. The root mean square (*rms*) of the velocity fluctuations

are determined by initially averaging 1199 instantaneous velocity vector fields and then determining the 1199 instantaneous fluctuating velocity vector fields. Figure 5 (streamwise,  $u'_{rms}$ ) and Figure 6 (cross stream,  $v'_{rms}$ ) illustrate the variation and scatter of peak values of *rms* velocity fluctuations in the plane wake of a cylinder over a wide range of Reynolds number from a variety of researchers. The magnitude of the peak velocity fluctuations from the current experimental observations ( closed square) agrees with the overall trend indicated by the comparison of experimental results obtained from Govardhan and Williamson (2001), Norberg (1986), and Konstantinidis, Balabani, and Yianneskis (2003).

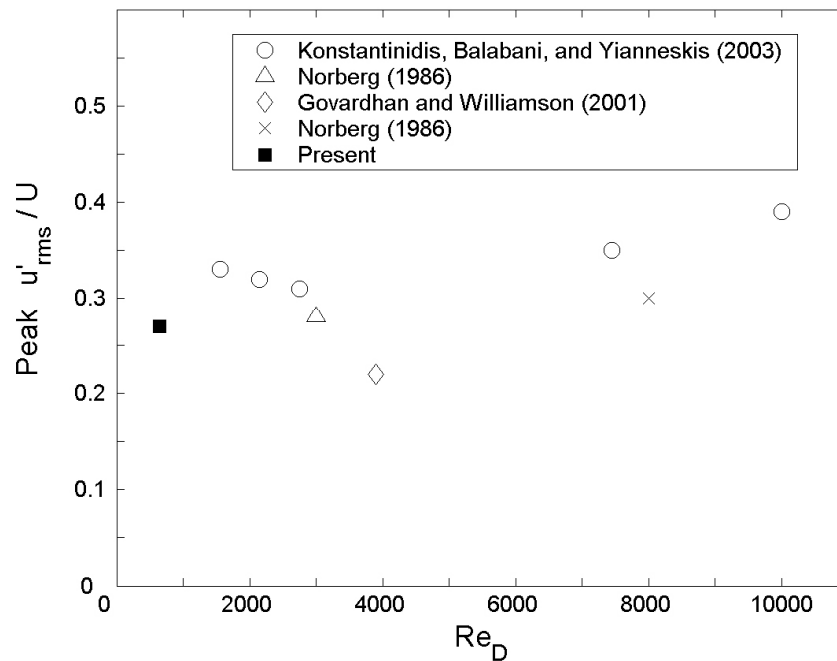


Figure 5. Comparison of streamwise peak values  $u'_{rms}$  of the current experiment with experimental data from other researchers for a wake from a cylinder.

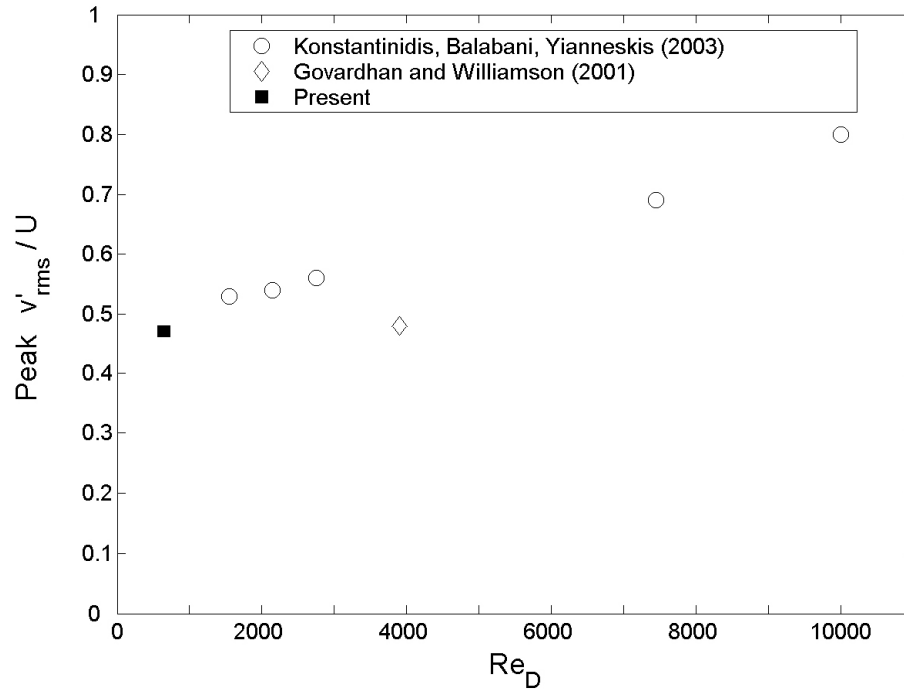


Figure 6. Comparison of cross stream peak values  $v'_{rms}$  of the current experiment with experimental data from other researchers for a wake from a cylinder.

The scatter seen in Figures 5 and 6 is expected as there are many factors that can affect the vortex shedding and formation of the near wake. Some of these factors are the cylinder surface, cylinder aspect ratio, free stream turbulence levels, and cylinder end conditions (Williamson 1996). The consequence of choosing a cylinder aspect ratio and a cylinder end condition is to effect the shedding modes of the plane wake. Undesirable oblique shedding modes can arise from the interaction of a cylinder with the boundary layer forming on the flow channels walls (Williamson 1996). An oblique shedding mode will propagate toward the center of the channel interfering with the desired measurement of the parallel shedding mode from a cylinder. To minimize these effects, cylinder

aspect ratios greater than 10 were chosen and a gap of approximately 3 mm was maintained between the cylinder ends and channel walls. The presence of oblique shedding modes was examined using dye traces initiated along the cylinder surface. Although the interaction of the cylinder and wall boundary layer could be seen, the effect on the overall flow appeared minimal. The propagation of dye traces initiated at the ends of the cylinder failed to travel towards the center of the channel at a significant rate. In addition velocity and density measurements were taken only in the center of the near wake directly behind the cylinder, before oblique shedding modes which might exist can affect the measured results.

In summary visualization of the wake by means of Nigrosene dye illustrates the periodic, turbulent nature of the wake. In addition an investigation of the vector field and vorticity behind the wake shows the expected appearance of shear layers and roll-up of vortices as measured through PIV. Finally, comparison of the peak *rms* velocity fluctuations with published experimental results appears to confirm the validity of the experimental setup and measurement techniques employed for this investigation.



#### 4. OBSERVATIONS

Visualizations of the wake are performed using Nigrosene dye to mark the fluid in the top water stream. Digital images are captured for: (A) a typical buoyancy-driven mixing layer; (B) a buoyant wake developing inside the mixing layer; (C) a wake with stable buoyancy; and (D) a wake excluding the effects of buoyancy. From photographs of these experiments, observations are presented comparing the behavior of the different wakes.

Digital images obtained from three separate experiments with Nigrosene dye added to the cold (top) water stream, are shown in Figure 7. Figure 7(A) shows a mixing layer driven by the Rayleigh-Taylor instability and Figure 7(B) shows the development of the same mixing layer as Figure 7(A) with a wake introduced into the mixing layer by a 1.6 cm diameter cylinder. Similarly Figure 7(C) uses a 3.25 cm diameter cylinder inserted into the center of the mixing layer. Comparison of Figure 7(C) with 7(A) reveals that the cylinder has introduced a dominant wake wavelength into the turbulent mixing layer behind the cylinder. The same effect is observed in Figure 7(B), however, is not as well defined. This long wavelength disturbance corresponds to the shedding frequency associated with the cylinder wake. Inspection of Figures 7(B) and 7(C), just upstream of the cylinder, reveals that the cylinder begins to redirect the flow approximately one cylinder diameter upstream. In particular, Figure 7(C) shows a large structure flowing around and off the bottom of the cylinder, associated with an induced wake flow.

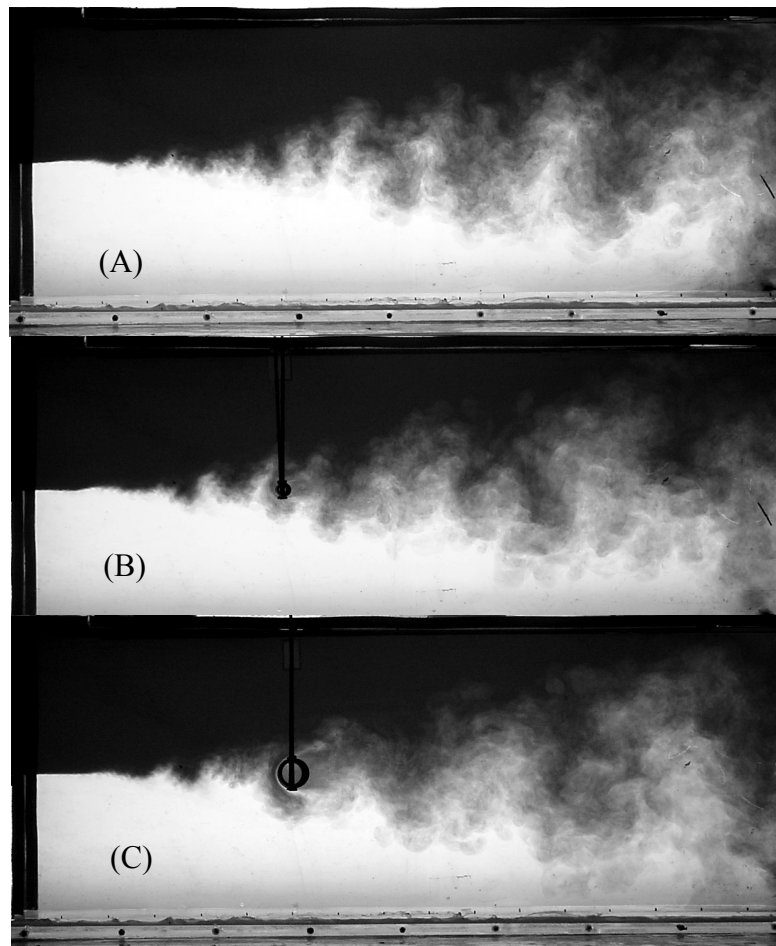


Figure 7. Visualizations of the buoyancy driven wake using Nigrosene dye. (A) Buoyancy driven-mixing layer (B) Buoyancy-driven mixing layer and wake with a cylinder of  $D = 1.6$  cm (C) Buoyancy-driven mixing layer and wake with a cylinder of  $D=3.25$  cm.  $U = 4$  cm/s for all three experiments.

Further comparison of Figures 7(A) and 7(B) indicates the wake formed behind the small diameter cylinder appears to have little or no effect on the overall mixing layer width. Comparing Figure 7(A) with 7(C), shows that a larger wake disturbance has

enhanced the overall growth rate of the mix region. This is consistent with the description of the evolution of a buoyancy-driven layer presented by Youngs (1984). In later stages of the mixing layer, the growth rate of smaller wavelength perturbations reaches a maximum due to the stabilizing effects of viscosity, while the growth rate of longer wavelength perturbations continues to increase. Generally these longer wavelengths evolve from the non-linear interaction of smaller wavelengths or bubble competition. As this process continues, large scale structures grow in size as viscosity is unable to affect their growth. In this limit, memory of the initial conditions for the mixing layer is lost and the mixing layer grows by  $h = \alpha A g t^2$ , where  $\alpha = 0.07$  for the water channel experiment (Snider and Andrews 1994). However, Youngs (1984) indicates that if a large amplitude, long wavelength perturbation originates in the flow by means other than bubble competition, the growth rate will exceed that predicted by  $h = \alpha A g t^2$ . In this experiment, a large amplitude long wavelength disturbance is introduced by the cylinder to the mixing layer once self-similarity is reached, and is not a remnant of the initial conditions.

Further insight into this behavior can be found by considering a single dominant growing wavelength,  $l_d$ , which drives the growth of the mixing layer. The value of  $l_d$  is determined by approximating the centerline vertical velocity by the terminal velocity of the dominant wavelength (Andrews and Spalding 1990) as

$$v' \sim 0.7 \sqrt{A g l_d / 2}. \quad (3)$$

The dominant wavelength can then be determined directly from the flow conditions and the centerline vertical velocity fluctuations. Using PIV measurements of the centerline

vertical velocity fluctuations approximately one diameter upstream of the cylinder, a dominant wavelength of  $l_d = 7 \text{ cm}$  is found. This magnitude is comparable to the wavelength of the disturbance created by the cylinder in Figure 7(B) of approximately 8 cm. Even though the dynamics of the turbulence in the mixing layer are affected by the wake, the overall growth of the mixing layer remains generally unaffected by the wake. In contrast, the large diameter cylinder of Figure 7(C) clearly alters the growth of the buoyancy-driven mixing layer. The large diameter cylinder introduces a long wavelength disturbance of approximately 16 cm. This is approximately twice the size of the dominant wavelength created by the buoyancy driven turbulence. As a result, it is expected the growth of the mixing layer would no longer follow the self-similar behavior defined by  $h = \alpha A g t^2$ , where  $\alpha = 0.07$ . This analysis is in agreement with the observations from Figure 7.

It is of interest to examine the structure of the buoyant wake. The usual wake structures of alternating regions of opposite sign vortices associated with a vortex street are not readily apparent in Figures 7(B) and 7(C). This is first attributed to the observed turbulence in the wake; however, a well defined vortex sheet is expected for wakes behind a cylinder even at a very large  $Re$  (Williamson 1996). The similarity of Figure 7(B) and 7(C) with the pure buoyancy case of 7(A) suggests that small scale structures are either being driven by the buoyancy, or are artifacts from the buoyancy-driven mixing layer before the cylinder. It is evident in Figures 7(B) and 7(C) that far downstream, on the right side of the images (greater than  $15 D$ ), the structures appear very similar to the Rayleigh-Taylor instability structures seen on the right of Figure 7(A).

All these observations suggest that buoyancy has quickly resumed a dominate role downstream of the cylinder.

PLIF images taken in the near field of the wake are shown in Figure 8. The initial development of the unstably stratified wake with  $U = 4$  cm/s,  $D = 1.6$  cm, and  $A = 5 \times 10^{-4}$  is shown. The interrogation window for these images is 10.5 cm x 8.4 cm at a resolution of 1000 x 800 pixels. The capture of a single image plane allows for clearer observation of the near field dynamics. The cold water stream is marked by fluorescent dye, while the hot water stream appears black. The cylinder is located just outside the field of view on the left side of the image, centered vertically. A small roll-up of a vortex is seen behind the cylinder in Figure 8(A). Downstream however, turbulent mixing from the Rayleigh-Taylor instability appears to have prevented the progression of a vortex street from the back of the cylinder. Mushroomed shaped plumes associated with the Rayleigh-Taylor instability are seen throughout the field of view. The shedding of vortices behind the cylinder are more evident in Figure 8(B), as a shed vortex can be seen moving away of the cylinder near the center of the image. On the far right side of the image, a pair of vortices shed from the cylinder can still be faintly observed. From these images it is clear that vortices are shed from the cylinder in a similar manner as for a non-buoyant wake. The buoyancy driven turbulence however quickly overwhelms the wake dynamics.

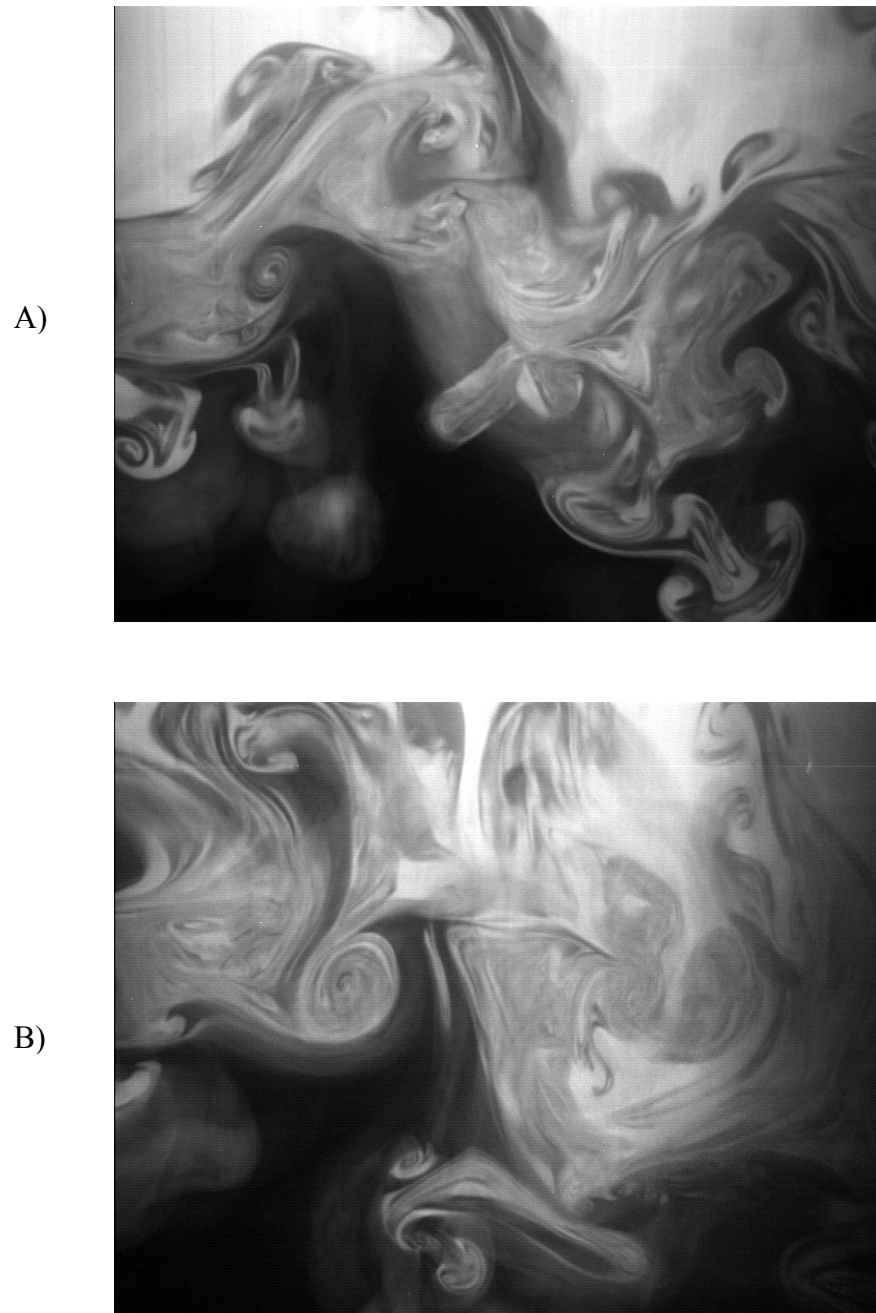


Figure 8. PLIF images in the near field of an unstably stratified wake.

An additional comparison concerning the effects of buoyancy on the wake can be made from visualizations shown in Figure 9. Figure 9(A) is the buoyant wake previously shown in Figure 7(B) and Figure 9(B) is the same wake except the stratification has been reversed. A stable stratification has been produced by introducing the hot water stream (marked by the Nigrosene Dye in Figure 9(B)) above the cold water stream. The expected effect of stable stratification on the wake is to inhibit the turbulent motions in the vertical direction, inhibiting growth of the wake. Figure 9(C) shows the canonical case of the wake behind a cylinder without the effects of buoyancy. All three visualizations shown in Figure 9 use a cylinder diameter of 1.6 cm. Clearly the behavior of the buoyant wake is very different from both the wake with stable buoyancy and without buoyancy.

Upon examination of Figure 9(C), the expected vortex street for a cylinder wake and turbulent nature of the vortices shed are apparent. A shear layer shed from top of the cylinder can be seen rolling-up into vortices approximately  $3 D$  behind the cylinder. This near wake behavior is similarly seen for the wake with stabilizing buoyancy shown in Figure 9(B). The very near wake region (less than  $5 D$ ) of the stably stratified wake appears to develop independent of the buoyancy. This is in agreement with observations of Bonnier and Eiff (2002) who examined the axisymmetric wake in a stably, continuously

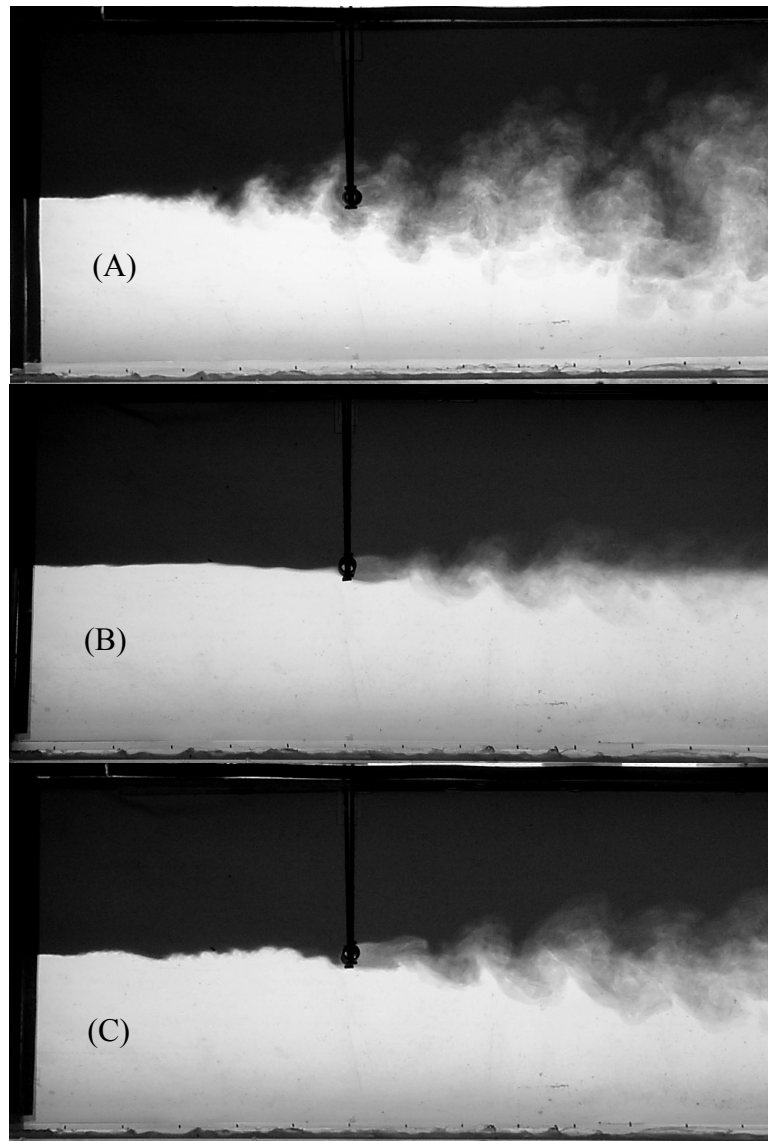


Figure 9. Visualizations of buoyancy effects on wakes using Nigrosene dye. (A) Buoyant wake (B) Wake with stabilizing buoyancy (C) Wake without buoyancy effects. All three wakes are formed from flow around a cylinder of  $D = 1.6$  cm and  $U = 4$  cm/s.



stratified fluid. However, downstream the stably stratified wake of Figure 9(B) stops growing in the vertical direction and the small scale motion appears to damp out, in contrast with the canonical no buoyancy case of Figure 9(C). The stabilizing effects of buoyancy hasten the collapse and decay of the wake. As previously mentioned, shedding from the cylinder is only weakly defined for the buoyant wake shown in Figure 9(A). In addition the formation region for the wake and the roll-up of vortices is not as apparent, especially when compared with Figures 9(B) and 9(C). Unstable buoyancy enhances the small scale structure and growth of the wake, providing a continuous source of energy for the wake and the mixing layer.

## 5. EXPERIMENTAL DATA AND ANALYSIS

### 5.1 Vertical velocity fluctuations in the near wake

The behavior of the vertical velocity fluctuations are of particular interest when considering the effects of buoyancy on the developing wake. Both stable and unstable buoyancy directly effect the vertical motion of the turbulence in the wake behind the cylinder. A quantitative comparison of *rms* vertical velocity fluctuations measured using the PIV technique previously described follows.

Figure 10 shows the measured  $v'_{rms}$ , taken at the centerline of the wake for experiments using the 1.6 cm diameter cylinder. Inspection of Figure 10 reveals several interesting and immediate observations in the far field  $x/D$  greater than 6. In particular, comparison of the unstable buoyancy case (squares) with the no buoyancy case (circles) shows that, as expected, the unstable buoyancy feeds potential energy into the vertical velocities and overcomes the dissipative nature of the wake. In contrast, stable buoyancy vertical velocity fluctuations (triangles) are suppressed and decay faster than in the no buoyancy case (circles) in the region behind the cylinder. The competition between dissipation and potential energy release is seemingly balanced at about 6 diameters downstream, however it is likely that this fixed point is due to the equal and opposite flow parameters of  $Fi^2 = \pm 7$  and corresponding  $A = \pm 5 \times 10^{-4}$ .

Figure 10 also shows the growth of vertical velocity fluctuations for a mixing layer driven by the Rayleigh-Taylor instability only (dashed line). Vertical velocity

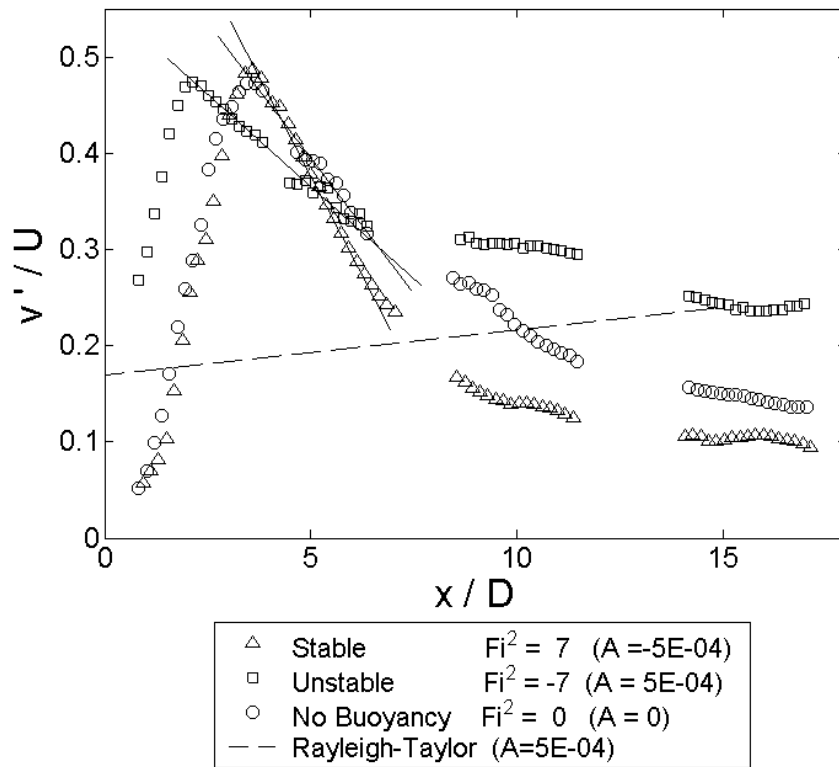


Figure 10. Decay of vertical velocity fluctuations,  $v'_{rms}$ , in the wake of a cylinder with stable buoyancy (triangles), unstable buoyancy (squares), no buoyancy (circles), and a typical Rayleigh-Taylor mixing layer for the same experimental conditions (dashed line).

fluctuations in the wake with unstable buoyancy (squares) clearly converge towards the equilibrium behavior of the buoyancy-driven mixing layer (dashed line) at approximately  $15 D$  downstream of the cylinder. It is apparent the strong wake dissipation observed in the no buoyancy case is quickly overcome by the unstable buoyancy. An argument could be made that if a wake could introduce very large wavelengths in the mixing layer, the release of potential energy to the turbulence could be enhanced. The larger scales would release increasing amounts of potential energy stored by means of the unstable stratification in the surrounding flow. This would result

in an increased growth rate for the mixing layer and centerline  $v'_{\text{rms}}$ . However as Figure 10 shows, measurements of  $v'_{\text{rms}}$  for the wake with unstable buoyancy recovers to a value approximately equivalent to that of pure buoyancy-driven turbulence. Implying the disturbance introduced by the cylinder with  $D = 1.6$  cm, is not sufficient to affect the rate at which energy is supplied to the developing mixing layer.

Now the very near field results for  $x/D$  less than 6 will be discussed and are shown in Figure 11. The left side of Figure 11 shows that the unstable buoyancy case (squares) starts with an initially higher level of vertical velocity fluctuation, this is due to the Rayleigh-Taylor mixing layer formed upstream of the cylinder. The peak vertical velocity for the no buoyancy and stable buoyancy cases occur at approximately the same location,  $x/D \sim 3.5$ , as might be expected because the wake dominates in the near cylinder region. This was previously seen in visualizations of the wake shown in the *Observations* section. However, for the wake with unstable buoyancy the peak velocity occurs at  $x/D \sim 2$ . This apparent discrepancy is attributed to the high momentum transport near the cylinder due to the upstream (prior to the cylinder) Rayleigh-Taylor mixing layer. The similar peak values for the three cases reflects similar wake dynamics, but the shift in the peak indicates that small scale mixing can significantly affect the overall development.

Variation in the location of this peak can be considered an indicator of variation in the length of formation for vortices shed from the cylinder (Konstantinidis *et al.* 2003). Although there have been many definitions for this length, all seem to describe the location of maximum vortex strength (Griffin 1995). According to Griffin, entrainment

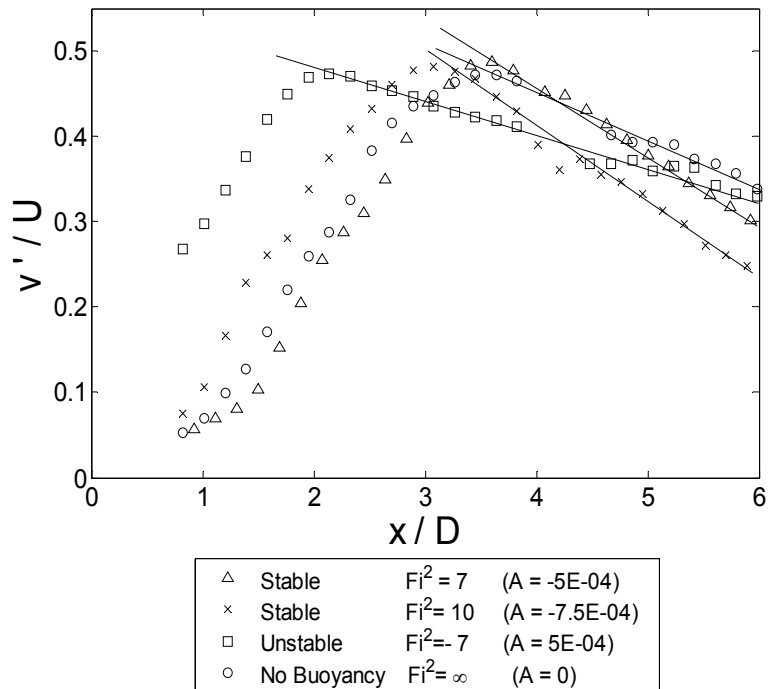


Figure 11. Decay of vertical velocity fluctuations,  $v'_{rms}$ , in the very near wake of a cylinder with stable buoyancy, unstable buoyancy, and no buoyancy.

of the separating shear layer feeds the growing vortex until it is strong enough to draw the opposing shear layer towards itself. The opposite vorticity of the opposing shear layer then prevents the vortex from growing further and the vortex is finally shed from the cylinder. Conceivably if entrainment of fluid into the vortex is increased the formation region will shorten and peak velocity fluctuations will occur closer to the cylinder. This effect is seen with increasing  $Re$  in the range of  $10^3$ - $10^4$  from experiments by Unal and Rockwell (1988) for the wake with no buoyancy.

In a similar manner the unstable buoyancy and its associated upstream mixing layer may increase entrainment of fluid into the forming vortex for the buoyant wake, causing the vortex to shed closer to the cylinder. To further investigate this possibility, Figure 12 shows the peak location of the  $v'_{\text{rms}}$  measured for two experiments with unstable buoyancy under the same flow conditions. Initially the cylinder is located 25 cm downstream of the splitter plate and then again at 35 downstream. Turbulence levels prior to the cylinder are higher when the cylinder is at 35 cm than at 25 cm as the mixing layer has had more time to evolve. This is illustrated by the initial values of  $v'_{\text{rms}} / U$  behind the cylinder. As expected the peak location of the  $v'_{\text{rms}}$  occurs closer to the cylinder as shown in Figure 12. Indicating the formation region of the wake has shortened from the increased levels of turbulence prior to the cylinder and the resulting increase in momentum transport behind the cylinder.

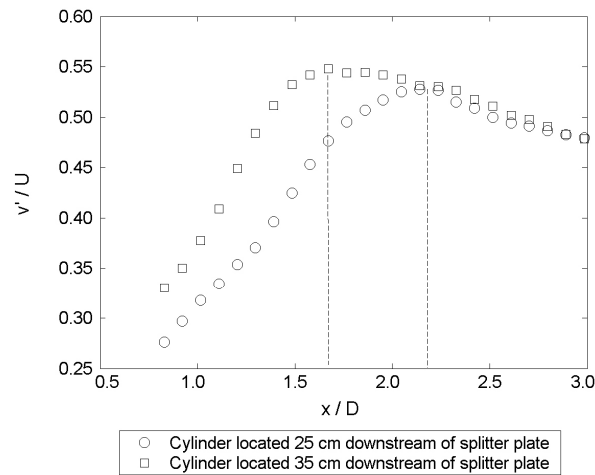


Figure 12. Variation of the location of peak  $v'_{\text{rms}}$  with mixing layer turbulence level. Flow conditions for both cases were with a  $U = 4.4$  cm/s,  $A = 5 \times 10^{-4}$  and  $D = 1.6$  cm.

Returning to Figure 11 and considering the subsequent decay in the vicinity immediately after the peak velocity. An apparent linear decay for each case is seen but with different slopes. The steepest slope, and hence the greatest decay, is for the stable buoyancy case. This is readily attributed to the stabilizing effect of the density stratification. The lowest slope is for the unstable buoyancy case, and is attributed to the release of potential energy from the unstable density stratification feeding into the kinetic energy of the flow, and thus the vertical velocity fluctuations. Additional slopes have been measured and are reported in Table 2. The gradients have been non-dimensionalized with the wake shedding frequency  $U/D$  to be compared with a model for the decay of turbulence kinetic energy described in a subsequent section.

	<b>Stratification</b>	$A$	$Fi^2$	$Re_D$	$D$ (cm)	$U$ (cm/s)	$(\partial v'/\partial x)(D/U)$
(1)	Stable	$-7.5 \times 10^{-4}$	10	630	1.6	3.9	-0.085
(2)	Stable	$-5 \times 10^{-4}$	7	630	1.6	3.9	-0.077
(3)	None	0	$\infty$	640	1.6	4.0	-0.054
(4)	Unstable	$5 \times 10^{-4}$	-7	690	1.6	4.3	-0.038
(5)	Unstable	$7.5 \times 10^{-4}$	-10	640	1.6	4.0	-0.061
(6)	Stable	$-5 \times 10^{-4}$	7	380	0.94	4.0	-0.074
(7)	None	0	$\infty$	380	0.94	4.0	-0.024
(8)	Unstable	$5 \times 10^{-4}$	-7	370	0.94	3.9	-0.043

Table 2. Summary of decay rates of vertical velocity fluctuations.

The  $v'_{\text{rms}}$  decay rates of cases (1)-(4) show the expected behavior from the effects of buoyancy. However case (5), where higher unstable density gradients result in increased levels of turbulence before the cylinder, the  $v'_{\text{rms}}$  decay rate is actually faster than case (4) where the unstable density gradients are smaller. In addition, case (7) where there is no buoyancy shows a slower decay of  $v'_{\text{rms}}$  than when unstable buoyancy is present as in case (8). This wake may be behaving in a transitional regime where it is not fully turbulent at such a low Re.

### 5.2 Molecular mixing in the near wake

In addition to the described velocity measurements, *rms* density fluctuations were obtained at the centerline of the wake using the high-resolution thermocouple system described previously. The recorded centerline density fluctuations are used to evaluate the extent of molecular mixing inside the wake. To evaluate molecular mixing the following parameters are defined (Ramaprabhu and Andrews 2004):

$$\begin{aligned}
 f_1 &= \lim_{T \rightarrow \infty} \frac{1}{T} \int_0^T \frac{\rho - \rho_2}{\rho_1 - \rho_2} dt \\
 f_2 &= 1 - f_1 \\
 B_o &= \lim_{T \rightarrow \infty} \frac{1}{T} \int_0^T (\rho - \bar{\rho})^2 dt / \Delta\rho^2 \\
 B_2 &= f_1 f_2 \\
 \theta &= 1 - \frac{B_o}{B_2}
 \end{aligned} \tag{4}$$

The volume fractions of the cold and hot fluids inside the wake are given by  $f_1$  and  $f_2$ .  $B_o$  is the intensity of the turbulent density fluctuations and  $B_2$  is the same



measure if the two streams were completely immiscible. The level of molecular mixing is evaluated through the molecular mix parameter,  $\theta$ . For two completely molecular mixed fluids  $\theta$  is equal to 1 and for two immiscible fluids  $\theta$  is 0 (Youngs 1990).

Figure 13 shows the molecular mix parameter,  $\theta$ , behind the cylinder for the unstable (squares) and stable (circles) stratifications with  $A=5 \times 10^{-4}$ ,  $-5 \times 10^{-4}$  respectively. In addition the levels of molecular mix found typically in a Rayleigh-Taylor mixing layer are shown (diamonds) (Ramaprabhu and Andrews 2004). Directly behind the cylinder it is readily seen that  $\theta$  is close to 1 for both the stable and unstable stratifications. This is due to the recirculation region immediately behind the cylinder. In both instances the level of molecular mixing decreases rapidly beyond the recirculation region. However, the unstable case quickly approaches an approximately constant value

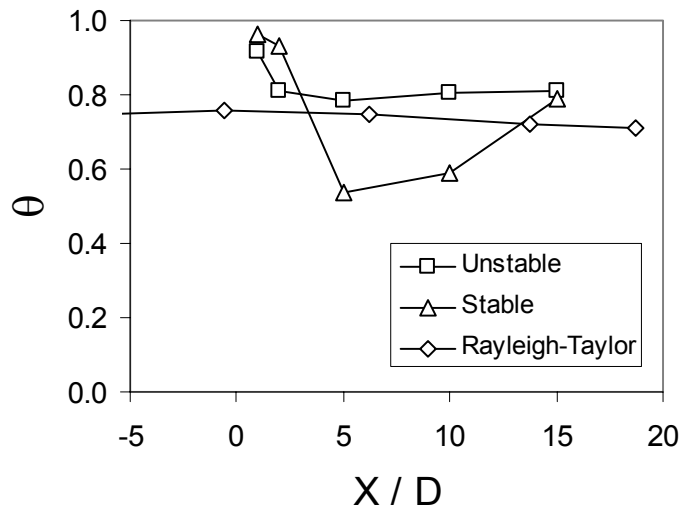


Figure 13. Evolution of the molecular mix parameter,  $\theta$ , in the near wake. Measured from centerline density fluctuations. Data for the Rayleigh-Taylor mixing layer obtained from Ramaprabhu and Andrews (2004).

of  $\theta = 0.8$ . In contrast the wake with stable buoyancy continues to decrease to a minimum of  $\theta = 0.54$  at  $5 D$ . However, far downstream of the cylinder at  $15 D$ , both the stable and unstably stratified wakes approach similar levels of molecular mixing. Thermal diffusion, enhanced by the dynamics of the turbulent wake, results in an increase of the mixing in the stably stratified wake. The dramatic reduction in the molecular mixing seen initially illustrates a counter gradient effect. A comparison can also be made between the typical Rayleigh-Taylor mixing layer (diamonds) and the instance when a wake is introduced (squares), similar behavior and magnitudes of molecular mix are seen in Figure 13. Both the mixing layer and unstably stratified wake show an approximately constant value of  $\theta$  as they evolve. The larger value of  $\theta$  for the unstably stratified wake is indicative that the cylinder and the subsequent wake contributes to the molecular mixing inside the buoyancy driven mixing layer.

Similarity between molecular mixing of the wake with unstable buoyancy and the Rayleigh-Taylor mixing layer can also be seen in power spectra of density fluctuations at the centerline of the wake and mixing layer, shown in Figure 14. Both measurements are obtained at approximately the same point of evolution of the buoyancy driven turbulence and the spectra is smoothed through a window averaging technique for clearer comparison. To make this comparison a non-dimensional time is defined as (Ramaprabhu and Andrews, 2004),

$$T = \frac{x}{U} \left( \frac{Ag}{H} \right)^{1/2} \quad (5)$$

where  $x$  is the distance downstream from the splitter plate,  $U$  is the free stream velocity,

$A$  is the Atwood number,  $g$  is the acceleration due to gravity, and  $H$  is the depth of the water channel. The power spectra of density fluctuations shown in Figure 14 for a self-similar Rayleigh-Taylor mixing layer were obtained from Ramaprabhu (2003) for  $T = 1.47$ . The power spectra of density fluctuations for the wake with unstable buoyancy are measured at a non dimensional time of  $T=1.42$ , which corresponds to  $10 D$  behind the cylinder. The power spectra is non-dimensionalized by the channel depth  $H$  and the wavenumber is determined from frequency using the convective velocity  $U$  which is approximately 4 cm/s. Even though the wake was introduced into the mixing layer, the power spectra of the centerline density fluctuations demonstrate a similar distribution of energy compared with the pure Rayleigh-Taylor mixing layer. However it is apparent

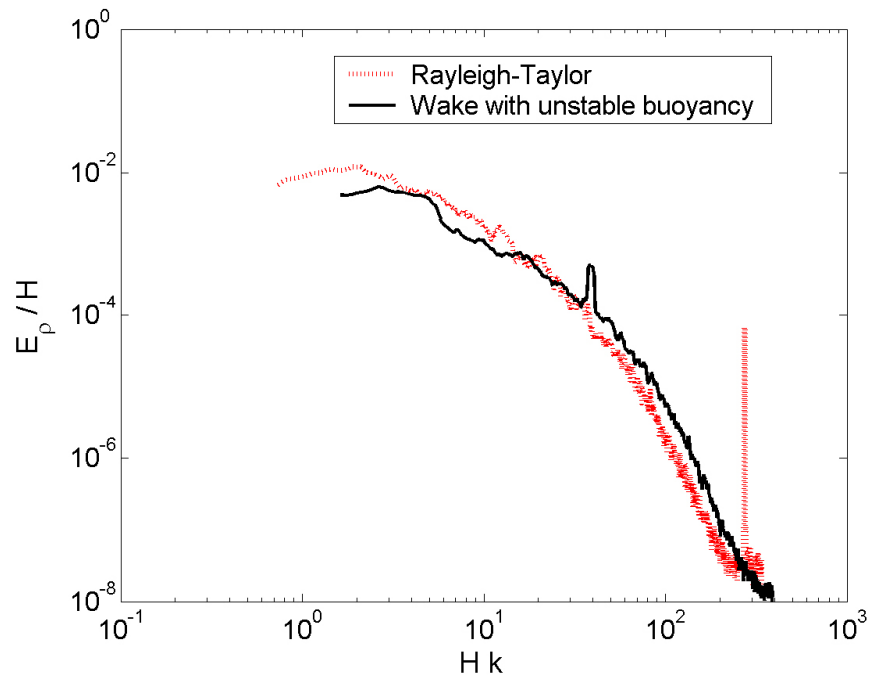


Figure 14. A comparison of power spectra of centerline density fluctuations in the buoyant wake (solid black line) and a mixing layer driven by the Rayleigh-Taylor instability (dotted red line) obtained from Ramaprabhu (2003).

that the wake has caused a transfer of energy of for the density fluctuations from large wavenumbers to small wavenumbers. From Figure 14, more energy can be seen at high wavenumbers for the wake with unstable buoyancy when compared to the Rayleigh-Taylor mixing layer. This confirms the enhanced molecular mixing measured in the wake with unstable buoyancy. A peak is seen in the power spectra for the wake with unstable buoyancy and is believed to be a harmonic of the wake shedding frequency. A peak is also observed in the power spectra for the Rayleigh-Taylor mixing layer, however it is likely noise.

As previously stated, the near wake dynamics seem to improve molecular mixing in the mixing layer, as shown by the slight increase in  $\theta$ . The distribution of length scales, as indicated by the density fluctuation power spectra, is similar to the Rayleigh-Taylor mixing layer. However higher energy levels in the large wavenumber fluctuations also indicates an improvement in molecular mixing compared with the Rayleigh-Taylor mixing layer.

### *5.3 Recovery of the buoyancy-driven turbulence*

Recovery of buoyancy-driven turbulence can be seen by examining  $\alpha$ , the growth constant for the mixing layer. The evolution of  $\alpha$  can be determined from the centerline  $v'_{\text{rms}}$  through the mix width by

$$v' = \frac{dh}{dt} = 2\alpha A g t. \quad (4)$$

The growth constant can then be computed as  $v'/2Agt$  as shown in Figure 15. The dashed line shows the expected value of 0.07 for  $\alpha$  (Snider and Andrews 1994).

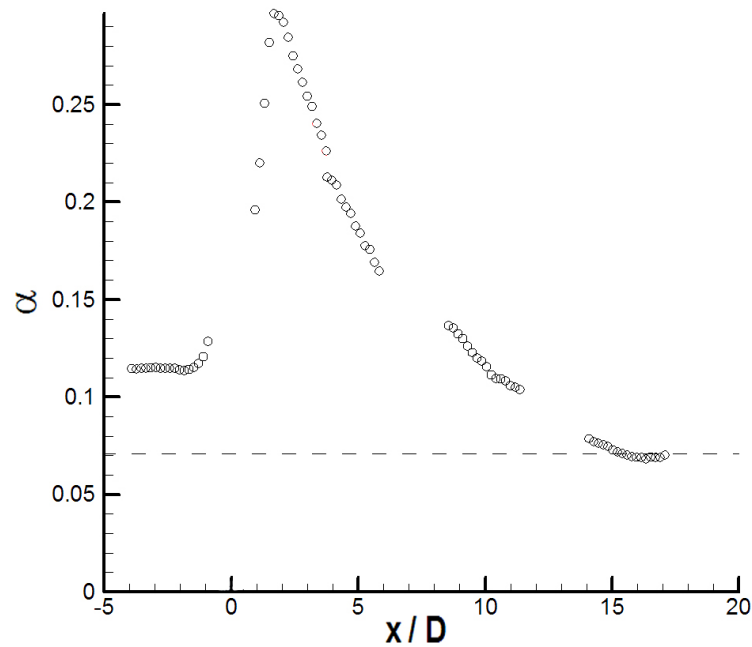


Figure 15. Demonstration of the recovery of buoyancy driven turbulence through the determination of  $\alpha$  from  $v'/2Agt$ .

The wake dynamics preclude an accurate representation of the growth constant in this manner in the very near wake. In addition an effect of the wake upstream of the cylinder can be seen as  $\alpha$  is a constant 0.12. However, from Figure 15 it is evident that at  $15 D$  downstream from the cylinder,  $\alpha$  does return to an approximately constant value of 0.07 associated with the buoyancy driven turbulence. This is an indication of the fast recovery to equilibrium behavior of the developing mixing layer and Rayleigh-Taylor instability. This recovery of the buoyancy driven turbulence is remarkably fast, when considering the usual dynamics of a wake where self-similarity is not reached until more than a hundred diameters downstream.

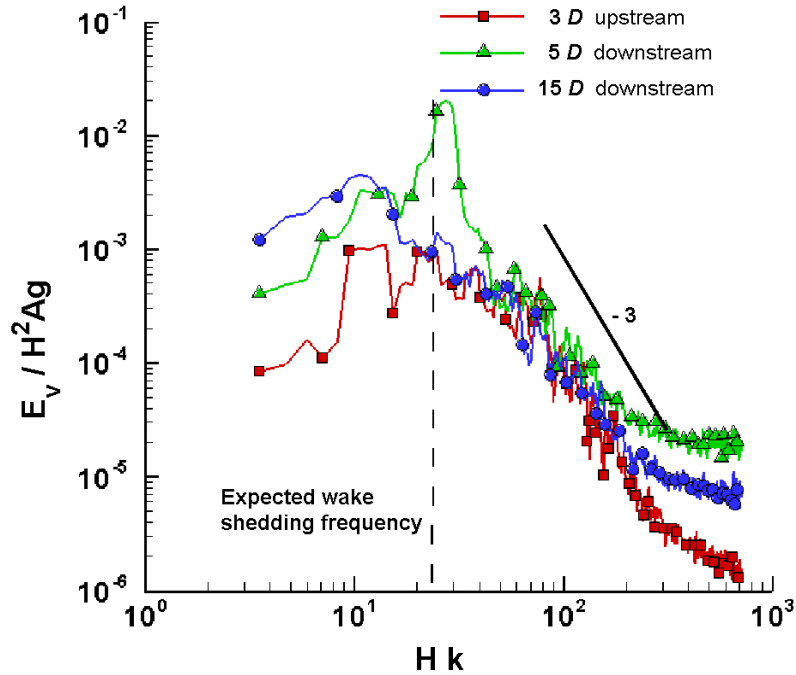


Figure 16. Power spectra of centerline  $v'$  in the buoyant wake for a cylinder diameter of 1.6 cm and  $A = 5 \times 10^{-4}$ .

Recovery of the buoyancy driven turbulence can also be observed through power spectra of centerline vertical velocity fluctuations in the buoyant wake as shown in Figure 16. The power spectra, shown as a function of wavenumber in Figure 16, is non-dimensionalized by the water channel depth ( $H$ ), the Atwood number ( $A$ ), and the gravitational acceleration ( $g$ ). A moving window average has been used to smooth the spectra to better illustrate the shape and slopes. The spectra is originally determined in a frequency domain and converted to wavenumber space using a convective velocity of 4 cm/s. Power spectra of the centerline vertical velocity fluctuations are shown at three locations relative to the cylinder of  $D = 1.6$  cm: in the mixing layer  $3 D$  upstream of the cylinder,  $5 D$  downstream of the cylinder, and  $15 D$  downstream of the cylinder. The

wake shedding frequency is clearly seen as a large peak in the power spectra of  $v'$  obtained 5  $D$  behind the cylinder. In addition the wake increases the energy contained in the vertical velocity fluctuations, particularly at large scales. Further downstream, 15  $D$  behind the cylinder, the distribution of energy of the  $v'$  is transitioning towards the spectra obtained in the Rayleigh-Taylor mixing layer prior to the cylinder. The peak in the spectra associated with the shedding frequency is no longer visible and the distribution of energy is similar to that of the power spectra obtained 3  $D$  upstream of the cylinder.

The power spectra of the vertical velocity fluctuations indicate the buoyancy driven turbulence has not completely recovered from the disturbance of the wake at 15  $D$ . It appears the power spectra is a better indicator of recovery than the overall magnitude of the  $v'_{rms}$  and  $\alpha$  from Figure 15, which would otherwise indicate a complete recovery of the buoyancy driven turbulence. From Figure 16 though, it is seen that the buoyancy driven turbulence is dominant, redistributing energy injected by the large scales of the wake as it transitions towards the self-similar behavior of the mixing layer. A measurement further downstream would have been acquired to confirm the complete return to a self-similar behavior of the energy distribution of the  $v'$ , but the mixing layer had grown to the limits of the channel dimensions.

## 6. A MATHEMATICAL MODEL FOR DECAYING VELOCITY FLUCTUATIONS IN THE NEAR FIELD OF A BUOYANT WAKE

A mathematical model is proposed for the decay of vertical velocity fluctuations in the near field of a buoyant wake. The model seeks to capture the dissipative nature of the wake, and the effects of density stratification on the near wake behavior once the velocity fluctuations have peaked. Solutions for the model are found for the wake with no buoyancy, with stable buoyancy, and unstable buoyancy. These solutions are then used to estimate decay rates of the vertical velocity fluctuations to be compared with those found experimentally.

A one-equation model for the transport of kinetic energy, as proposed originally by Kolmogorov and Prandtl, is modified to describe the transport of vertical velocity fluctuations in the near wake. The general transport model for kinetic energy is

$$\frac{Dk}{Dt} = \nabla \cdot \left( \frac{\nu_t}{\sigma_k} \nabla k \right) + P - \varepsilon \quad (6)$$

where  $k$  is kinetic energy,  $\nu_t = c_\mu k^{1/2} l_m$  is the turbulent viscosity,  $\sigma_k$  is the turbulent Prandtl number,  $P$  is the production of kinetic energy, and  $\varepsilon$  is dissipation. Expanding the substantial derivative yields

$$\frac{Dk}{Dt} = \frac{\partial k}{\partial t} + U \frac{\partial k}{\partial x} + V \frac{\partial k}{\partial y} + W \frac{\partial k}{\partial z}. \quad (7)$$

Since the flow in the water channel is statistically steady and the mean flow in directions other than the x-direction can be neglected, Eq. (7) simplifies to:



$$\frac{Dk}{Dt} = U \frac{dk}{dx}. \quad (8)$$

Assuming a “top-hat” profile for  $k$  across the wake (in the  $y$ -direction) then  $k = k(x)$  and the diffusion transport from the model equation,

$$\nabla \cdot \left( \frac{\nu_t}{\sigma_k} \nabla k \right) = \frac{\partial}{\partial x} \left( \frac{\nu_t}{\sigma_t} \frac{\partial k}{\partial x} \right) + \frac{\partial}{\partial y} \left( \frac{\nu_t}{\sigma_t} \frac{\partial k}{\partial y} \right) + \frac{\partial}{\partial z} \left( \frac{\nu_t}{\sigma_t} \frac{\partial k}{\partial z} \right), \quad (9)$$

is simplified to

$$\nabla \cdot \left( \frac{\nu_t}{\sigma_k} \nabla k \right) = \frac{d}{dx} \left( \frac{\nu_t}{\sigma_t} \frac{dk}{dx} \right). \quad (10)$$

These simplifications reduce the original model equation to

$$U \frac{dk}{dx} = \frac{d}{dx} \left( \frac{\nu_t}{\sigma_t} \frac{dk}{dx} \right) + P - \varepsilon. \quad (11)$$

The differential transport equation can also be written in integral form across the wake, where  $\delta$  is the width of the wake.

$$\int_{-\delta}^{\delta} \left( U \frac{dk}{dx} \right) dy = \int_{-\delta}^{\delta} \frac{d}{dx} \left( \frac{\nu_t}{\sigma_t} \frac{dk}{dx} \right) dy + \int_{-\delta}^{\delta} P dy - \int_{-\delta}^{\delta} \varepsilon dy \quad (12)$$

By dividing the entire equation by  $2\delta$ , the integral form the model equation can be rewritten as

$$U \frac{d}{dx} \frac{1}{2\delta} \int_{-\delta}^{\delta} (k) dy = \frac{1}{2\delta} \int_{-\delta}^{\delta} \frac{d}{dx} \left( \frac{\nu_t}{\sigma_t} \frac{dk}{dx} \right) dy + \frac{1}{2\delta} \int_{-\delta}^{\delta} P dy - \frac{1}{2\delta} \int_{-\delta}^{\delta} \varepsilon dy \quad (13)$$

$$U \frac{d\langle k \rangle}{dx} = \frac{1}{2\delta} \int_{-\delta}^{\delta} \frac{d}{dx} \left( \frac{\nu_t}{\sigma_t} \frac{dk}{dx} \right) dy + \langle P \rangle - \langle \varepsilon \rangle \quad (14)$$

The remaining diffusion term in the downstream direction is negligible compared with

the convection of turbulent kinetic energy. As seen in the *Observations* section from visualizations of the wake with unstable buoyancy, expansion of the wake in the y-direction behind the cylinder is small, this would seem to indicate that convection transport in the x-direction is much larger than diffusion transport in the x-direction. Assuming diffusion transport in the x-direction is negligible, the model equation is now written as

$$U \frac{d\langle k \rangle}{dx} = \langle P \rangle - \langle \varepsilon \rangle. \quad (15)$$

Using a high *Re* approximation, dissipation is modeled as  $\langle \varepsilon \rangle = C_D \langle k \rangle^{3/2} / l_m$ , where  $C_D$  is an empirical constant and  $l_m$  is a mixing length associated with dissipation. Production of turbulent kinetic energy is modeled as

$$\langle P \rangle = -\frac{\Delta\rho}{\rho} g \langle k \rangle^{1/2} \quad (16)$$

where  $\Delta\rho = \rho_1 - \rho_2$ , and  $g$  is the (-) acceleration due to gravity (Snider and Andrews 1996). For unstable stratification the quantity  $\Delta\rho$  is positive and for stable stratification is negative. Alternatively  $\langle P \rangle$  may be written in terms of the Atwood number,  $A = (\rho_1 - \rho_2) / (\rho_1 + \rho_2)$ , so that

$$\langle P \rangle = -2Ag \langle k \rangle^{1/2} \quad \text{from} \quad \frac{\Delta\rho}{\rho} = \frac{(\rho_1 - \rho_2)}{(\rho_1 + \rho_2)/2} = 2A \quad (17)$$

The kinetic energy transport model for the near wake can now be written as

$$U \frac{d\langle k \rangle}{dx} = -\frac{\Delta\rho}{\rho} g \langle k \rangle^{1/2} - \frac{C_D \langle k \rangle^{3/2}}{l_m}. \quad (18)$$

If the flow is assumed to be locally isotropic the kinetic energy can be related to the vertical velocity fluctuations by  $k = (3/2)(v')^2$ . Rewriting the kinetic energy transport

model of Eq. (18) in terms of the vertical velocity fluctuations and applying Taylor's Hypothesis,  $t = x/U$ , yields

$$\frac{dv'}{dt} = -\left(\frac{1}{6}\right)^{1/2} \frac{\Delta\rho}{\rho} g - \frac{3^{1/2}}{2^{3/2}} \frac{C_D v'^2}{l_m} \quad (19)$$

This form of the model is closely related to the two-fluid model proposed by Youngs (1984) for Rayleigh-Taylor mixing. The mixing length and the empirical constant  $C_D$  must be specified to close the model. The mixing length is typically chosen to be representative of the large scale motion (Rodi 1993). However there is little experimental data available on the appropriate selection of a mixing length. Presented by Rodi, Prandtl defines a mixing length by multiplying an empirically determined proportionality constant with the wake half width. It is also common to relate a mixing length to the mean velocity gradient,  $dU/dy$ , however from the symmetrical nature of the wake flow  $dU/dy = 0$  at the wake centerline (Rodi 1993) and so is not available. From observations, large scale motion of the wake is obviously related to the cylinder diameter through the shedding frequency. So for convenience, and due to the lack of experimental data on a more appropriate mixing length for a wake,  $l_m$  is taken to be the cylinder diameter,  $D$ . The empirical constant of  $C_D$  that appears in the dissipation term will be selected to match the experimental  $v'_{rms}$  decay rates. Assuming a local equilibrium for the potential energy and dissipation in the kinetic energy transport equation allows  $C_D$  to be estimated, and was found to be approximately 0.1 (Ng and Spalding 1972) for homogeneous shear flows. The dynamics of the near wake however are not in local equilibrium. Instead a different value of  $C_D$  is required to describe the

wake dissipation and match the experimentally determined  $v'_{rms}$  decay rates. Using the  $v'_{rms}$  decay rate for the wake with no buoyancy at  $Re = 640$  as a reference, the required  $C_D$  to capture the dissipation of the wake is 0.42, a factor of four times larger than the equilibrium value of 0.1. This higher value is attributed to the near field development of the wake we are studying.

The final form of the transport equation which is solved is as follows

$$\frac{dv'}{dt} = -\left(\frac{1}{6}\right)^{1/2} \frac{\Delta\rho}{\rho} g - \frac{3^{1/2} C_D v'^2}{2^{3/2} D} \quad (20 A)$$

$$\text{No buoyancy:} \quad \frac{dv'}{dt} = -\frac{3^{1/2} C_D v'^2}{2^{3/2} D} \quad (20 B)$$

$$\text{Stable buoyancy:} \quad \frac{dv'}{dt} = -\left| -\left(\frac{1}{6}\right)^{1/2} \frac{\Delta\rho}{\rho} g \right| - \frac{3^{1/2} C_D v'^2}{2^{3/2} D} \quad (20 C)$$

$$\text{Unstable buoyancy:} \quad \frac{dv'}{dt} = +\left| -\left(\frac{1}{6}\right)^{1/2} \frac{\Delta\rho}{\rho} g \right| - \frac{3^{1/2} C_D v'^2}{2^{3/2} D} \quad (20 D)$$

which can be rewritten more generally as

$$\frac{dv'}{dt} = av'^2 + bv' + c \quad (21)$$

With  $a = -\frac{3^{1/2} C_D}{2^{3/2} D}$ ,  $b = 0$ , and  $c = -\left(\frac{1}{6}\right)^{1/2} \frac{\Delta\rho}{\rho} g$ .

The assumptions made are:

- 1) The flow is statistically steady.
- 2) Mean velocity components in directions other than the x-direction can be neglected.
- 3)  $k$  follows a “top-hat” profile across the wake (in the y-direction) so that  $k = k(x)$ .
- 4) The diffusion transport term in the x-direction is negligible compared to convective transport in the x-direction.
- 5) The velocity fluctuations at the centerline of the wake are locally isotropic.

The form of the differential equation shown in Eq. (21) has general analytical solutions that can be found in mathematical reference books such as Abramowitz and Stegun (1972). Three distinct solutions can be obtained from Eq. (21) depending on whether the quantity  $(b^2 - 4ac)$  is positive, negative, or zero. This provides for three unique solutions corresponding to the decay of vertical velocity fluctuations in the wake with no buoyancy, with stable buoyancy, and the wake with unstable buoyancy. The solutions are listed in Eqs. (22-24). A detailed description of how these solutions are arrived at is shown in Appendix B.

Model Solutions:

No buoyancy: 
$$v' = \frac{1}{\left(-a t + \frac{1}{v'_{peak}}\right)} \quad (22)$$

Stable buoyancy: 
$$v' = \frac{(ac)^{1/2}}{a} \tan\left((ac)^{1/2} t + \arctan\left(\frac{a v'_{peak}}{(ac)^{1/2}}\right)\right) \quad (23)$$

Unstable buoyancy: 
$$v' = \frac{\left(\frac{-c}{a}\right)^{1/2}}{\tanh\left((-ac)^{1/2} t + \operatorname{arctanh}\left(\frac{\left(\frac{-c}{a}\right)^{1/2}}{v'_{peak}}\right)\right)} \quad (24)$$

Where  $a = -\frac{3^{1/2}}{2^{3/2}} \frac{C_D}{D}$ ,  $c = -\left(\frac{1}{6}\right)^{1/2} \frac{\Delta\rho}{\rho} g$ , and  $v'_{peak}$  is the maximum value of the  $v'_{rms}$  at the centerline of the near wake.

Figure 17 shows the behavior of each solution taking a constant mixing length of  $D$  and  $C_D = 0.42$ . In each case associated with the model equations 20 (B) – (D), an apparent linearity of the initial decay of the vertical velocity fluctuations can be seen as expected from the experimental results. This apparent linearity corresponds to a  $1/(a_o t + a_1)$  behavior (Eq. (22)) for the decay of the  $v'_{rms}$  from their peak values as also found in the experimental results, as shown in Figure 18. The curve fit,  $1/(a_o t + a_1)$ ,

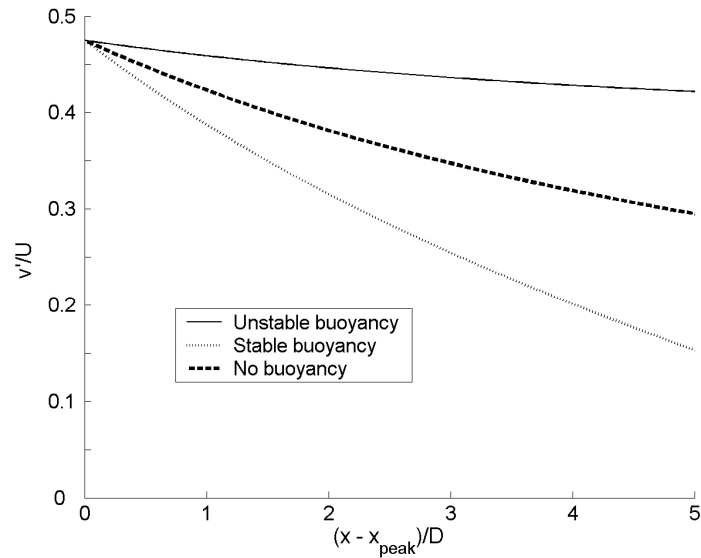


Figure 17. Decay of  $v'_{rms}$  in the near wake for the cases of no buoyancy, stable buoyancy, and unstable buoyancy as determined from the model solutions using  $C_D = 0.42$  and for  $A = \pm 5 \times 10^{-4}$ .

closely fits the experimental data. Discrepancies which are seen, approximately  $10 D$  downstream, are more likely due to variation in laser sheet intensity of the PIV system than a result of the flow conditions. As indicated by the model solution, unstable buoyancy decreases the decay rate of the  $v'_{rms}$  in the near wake. Conversely, stable buoyancy appears to increase the decay rate of  $v'_{rms}$ . If the density difference is reduced to very small values both the unstable and stable buoyancy solutions collapse onto the solution for the wake without buoyancy. Qualitatively the behavior of the model is remarkably consistent with the experimental results.

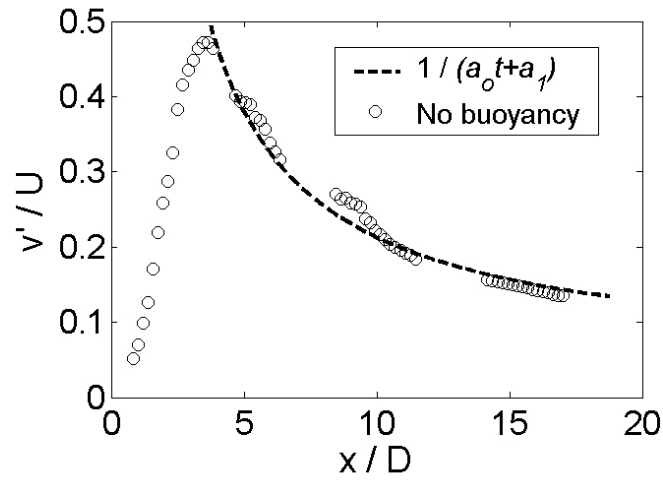


Figure 18.  $1/(a_0 t + a_1)$  decay of vertical velocity fluctuations in the near wake for a cylinder wake without buoyancy.

	Stratification	$A$	$D$ (cm)	$C_D$	$(\partial v'/\partial x)(D/U)$	
					Experiment	Model
(1)	Stable	$-7.5 \times 10^{-4}$	1.6	0.42	-0.085	-0.11
(2)	Stable	$-5.0 \times 10^{-4}$	1.6	0.42	-0.077	-0.092
(3)	None	0	1.6	0.42	-0.054	-0.054
(4)	Unstable	$5.0 \times 10^{-4}$	1.6	0.42	-0.038	-0.017
(5)	Unstable	$7.5 \times 10^{-4}$	1.6	0.42	-0.061	-0.010
(6)	Stable	$-5.0 \times 10^{-4}$	0.94	0.42	-0.074	-0.068
(7)	None	0	0.94	0.42	-0.024	-0.047
(8)	Unstable	$5.0 \times 10^{-4}$	0.94	0.42	-0.043	-0.026

Table 3. Comparison of  $v'$  decay rates for the transport model and experimental results using a  $C_D = 0.42$ .



Table 3 compares  $v'_{rms}$  decay rates for various experiments and the mathematical model using  $C_D = 0.42$ . A value of  $C_D = 0.42$  is chosen as it captures the decay of the  $v'_{rms}$  for the wake with no buoyancy with  $D = 1.6$  cm. The initial hypothesis was that the decay of the  $v'_{rms}$  could be thought of as a superposition of the dissipative nature of the wake and buoyancy effects. This would allow for a single value of  $C_D$  to satisfy all three solutions. Indeed, as can be seen from Table 3, the general trends of the experimental results are captured in the model using a single value of  $C_D = 0.42$ . However, comparing the experiment and model for case (5) the agreement is poor, this is attributed to increased levels of upstream turbulence. In addition experimental results for case (7), do not show as good agreement with the model. This discrepancy may be expected however due to the transitional behavior of the wake at the low  $Re$ .

	<b>Stratification</b>	$A$	$D$ (cm)	$C_D$	$(\partial v'/\partial x)(D/U)$	
					<b>Experiment</b>	<b>Model</b>
(1)	Stable	$-7.5 \times 10^{-4}$	1.6	0.20	-0.085	-0.085
(2)	Stable	$-5.0 \times 10^{-4}$	1.6	0.29	-0.077	-0.077
(3)	None	0	1.6	0.42	-0.054	-0.054
(4)	Unstable	$5.0 \times 10^{-4}$	1.6	0.59	-0.038	-0.038
(5)	Unstable	$7.5 \times 10^{-4}$	1.6	0.77	-0.061	-0.061
(6)	Stable	$-5.0 \times 10^{-4}$	0.94	0.58	-0.074	-0.074
(7)	None	0	0.94	0.20	-0.024	-0.024
(8)	Unstable	$5.0 \times 10^{-4}$	0.94	0.59	-0.043	-0.043

Table 4. Comparison of  $C_D$  for the mathematical model.

From observations drawn from Table 3 it is evident the empirical coefficient  $C_D$  should be different for each of the three stratifications. To demonstrate such a range of values for  $C_D$ , Table 4 shows the required value of  $C_D$  for each model to match the corresponding experimental result. When examining the higher  $Re$  results with  $D = 1.6$  cm, a trend can be seen where  $C_{D \text{ stable}} < C_{D \text{ none}} < C_{D \text{ unstable}}$ . In contrast, the low  $Re$  results with  $D = 0.94$  cm requires similar values of  $C_D$  for both the stable and unstable buoyancy cases to match experimental results. However, once again the discrepancy in behavior may be due to the transitional behavior of the wake at low  $Re$ . More experimental data is needed to further calibrate the model, however, it appears that an approximate relationship for the empirical constant  $C_D$  can be defined for its dependence on stratification. Using the results at the higher  $Re$  with  $D = 1.6$  cm, it would appear that  $C_{D \text{ stable}} \approx 0.5C_{D \text{ none}}$  and  $C_{D \text{ unstable}} \approx 1.5C_{D \text{ none}}$ .

Recovery of the buoyancy driven turbulence can also be compared for the experimental results and model. Using the model solution for unstable stratification, the downstream location where buoyancy driven turbulence recovers can be determined. At this location the dissipation of the wake and turbulent production from buoyancy are balanced,  $\partial v' / \partial x = 0$ . The  $v'$  transport equation is solved for the vertical velocity fluctuation required to achieve a balance of the dissipation and turbulent production. Solving the transport equation in this manner for  $D = 1.6$  cm,  $U = 4$  cm, and  $A = 5 \times 10^{-4}$  with  $C_D = 0.59$  yields  $v'/U = 0.33$ . This corresponds to the asymptotic limit of the unstable buoyancy model solution. The location where the unstably buoyancy is

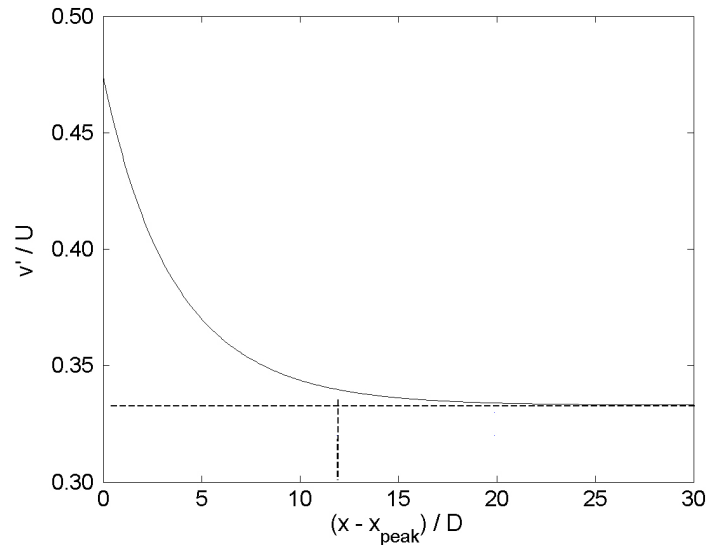


Figure 19. Recovery of buoyancy driven turbulence as demonstrated by the model solution for  $D = 1.6$  cm,  $U = 4$  cm, and  $A = 5 \times 10^{-4}$  with  $C_D = 0.59$ .

predicted to recover is found by determining where 95% of the total change of  $v'$  has been reached, as shown in Figure 19. From the model solution recovery of the buoyancy driven turbulence is found to occur  $11.9 D$  downstream of the peak value of  $v'_{rms}$ . Similarly, experimental results indicated a recovery approximately  $13 D$  downstream of the peak  $v'_{rms}$ . There is good agreement between the measured and predicted locations for the recovery of buoyancy driven turbulence. The turbulence levels at the point of recovery however show a discrepancy as the model indicates  $v'/U = 0.33$  and the experimental results showed  $v'/U = 0.23$ .

Clearly additional parameter variations and experimental results are required to correctly calibrate the proposed one equation model for vertical velocity fluctuations in the near wake of the cylinder. In addition, there may exist a mixing length other than the

diameter of the cylinder which better represents the flow. However, there is a general lack of experimental data in the near wake region of cylinder wake with unstable buoyancy to either calibrate  $C_D$  or estimate a mixing length for the flow. Even with these limitations, the proposed model was able to qualitatively demonstrate the observed effects of buoyancy on the decay of vertical velocity fluctuations in the near wake. In addition it was shown that by calibrating the empirical coefficient  $C_D$  the experimental decay rates of  $v'$  could be matched. Also the model prediction of the location downstream where buoyancy driven turbulence recovers shows good agreement with the experimental results.

## 7. CONCLUSIONS

A buoyant wake has been experimentally investigated in a water channel facility at Texas A&M University. A cylindrical obstruction placed at the centerline disturbs the equilibrium of a developing Rayleigh-Taylor mixing layer. The development of the near wake in the presence of unstable stratification is examined, and the recovery of the buoyancy driven mixing layer. Qualitative observations of the behavior are made through visualization of the mixing layer / wake interactions. Also, quantitative measurements of velocity fluctuations and density fluctuations in the near wake are obtained using PIV and a high resolution thermocouple system. The experimental measurements are used to investigate how the wake and buoyancy driven mixing layer interact. Additional experiments of the wake with no buoyancy and including stabilizing buoyancy are performed for comparison. Finally, a mathematical model is proposed to describe the response of velocity fluctuations in the near wake to the effects of buoyancy.

A summary of conclusions drawn from the experimental investigation of the mixing layer / wake interactions in the near field of the wake are as follows:

- The transport of energy to the wake from potential energy stored in the unstable density gradients, results in a remarkably rapid return to the characteristic behavior of the Rayleigh-Taylor mixing layer. Recovery of the buoyancy driven turbulence occurs approximately  $15 D$  downstream from the cylindrical obstruction where the centerline vertical velocity fluctuations return to the

characteristic magnitude and growth of the Rayleigh-Taylor mixing layer. Spectral measurements of the vertical velocity fluctuations show the redistribution of energy in the wake, and the progression of the energy distribution towards the characteristic behavior for buoyancy driven turbulence.

- The large scale growth of the mixing layer is largely unaffected by the cylinder wake primarily employed in this investigation. Visual observations however confirm that wake induced disturbances, larger than the characteristic length scale of the developing mixing layer, will increase the growth of the mixing layer.
- From visual observations of the unstably stratified wake and measurements of velocity fluctuations in the near field, the dynamics of the flow directly behind the cylinder is dominated by the wake, with little influence from the buoyancy. The decay of centerline velocity fluctuations in the very near wake, less than 6 diameters downstream, show an apparent linearity which decays by  $1/(a_0 t + a_1)$  for the wake without buoyancy. Stabilizing buoyancy increases the rate at which vertical velocity fluctuations decay compared to the canonical case of no buoyancy. However, unstable density gradients of the surrounding flow slow the decay of vertical velocity fluctuations in the near wake compared with the cases with stabilizing buoyancy or no buoyancy at all.

- The level of buoyancy driven turbulence preceding the cylinder and subsequent wake affects the length of the formation region for shedding vortices. Increases in the turbulence levels result in a shortening of the formation region. This is attributed to the high momentum transport near the cylinder from the upstream Rayleigh-Taylor mixing layer.
- Molecular mixing evaluated through density measurements at the centerline of the wake and mixing layer, shows a rapid return to an approximately constant value, similar to the expected behavior for a Rayleigh-Taylor mixing layer. However the dynamics of the wake and buoyancy driven turbulence result in an increase in the level of molecular mixing when compared with a typical Rayleigh-Taylor case.

Additional conclusions drawn from analysis of the mathematical model for the decay of vertical velocity fluctuations in the near field of the wake with unstable buoyancy are as follows:

- The proposed model qualitatively demonstrates the observed decay of centerline vertical velocity fluctuations in the near wake. Also it shows a decay of velocity fluctuations corresponding to a  $1/(a_0 t + a_1)$  behavior as seen from the experimental results. In addition, slower decay of vertical velocity fluctuations is found from the model solution for the unstably stratified wake. In contrast, the model solution for the stably stratified wake shows an increase in the decay

of vertical velocity fluctuations when compared with the wake with no buoyancy.

- The location downstream for recovery of the buoyancy driven turbulence predicted by the model shows good agreement with the experimentally measured result.
- Additional parameter variation and experimental results are recommended to further calibrate the proposed one-equation model for vertical velocity fluctuations in the near wake of the cylinder. In addition, further investigation is required to verify the selection of the cylinder diameter as the mixing length.

This experimental investigation in the near field of a cylinder wake in an unstably stratified flow is unique. As a result the investigation has been broad. The present study attempted to investigate the effects of a disturbance on the development of a Rayleigh-Taylor mixing layer, the interaction of the competing equilibria, and the effect of unstable buoyancy on the near wake development. As previously described in the literature review, study of wakes has been extensive. What limited research that exists about the effect of buoyancy on the wake dynamics has focused on the inclusion of stabilizing buoyancy. The difficulty in creating an unstably stratified flow has perhaps precluded investigations into the unstably stratified wake. Since there appears to be no significant research on this topic there are many opportunities for further study of dynamics in the unstably stratified wake. Some of which have been previously investigated in the wakes with stabilizing buoyancy and without buoyancy. Some



examples are the vortex structure under the effect of unstable buoyancy and the change in formation length for shedding vortices due to buoyancy driven turbulence. In addition, a parametric study of the buoyant wake could be performed to further characterize the behavior and development of the wake. The results of which would allow for proper calibration and improvements in the proposed mathematical model. The present research also might be extended to continue the investigation of the recovery of buoyancy driven turbulence to a disturbance of its equilibrium and the dynamics of the competing equilibria. This might lead to improvements of models of turbulence where a local equilibrium cannot be assumed.

## REFERENCES

- Abramowitz, M. and Stegun, I. 1972 *Handbook of Mathematical Functions with Formulas, Graphs, and Mathematical Tables*. Dover Publications.
- Adrian, R. J. 1997 Dynamic ranges of velocity and spatial resolution of particle image velocimetry. *Meas. Sci. Technol.* **8**, 1393–1398.
- Berger, E. and Willie, R. 1972 Periodic flow phenomena. *Ann. Rev. Fluid Mech.* **4**, 313-340.
- Bonnier, M. and Eiff, O. 2002 Experimental investigation of a turbulent wake in a stably stratified fluid. *Phys. Fluids* **14**(2), 791-801.
- Chandrasekhar, S. 1961 *Hydrodynamic and Hydromagnetic Stability*. Clarendon.
- Chang, K. and Sa, J. 1990 The effect of buoyancy on vortex shedding in the near wake of a circular cylinder. *J. Fluid Mech.* **220**, 253-266.
- Dimonte, G. and Schneider, M. 1996 Turbulent Rayleigh-Taylor instability experiments with variable acceleration. *Phys. Rev. E* **54**(4), 3740-3743.
- Govardhan, R., and Williamson, C.H.K. 2001 Mean and fluctuating velocity fields in the wake of a freely vibrating cylinder. *J. Fluids and Structures* **15**, 489-501.
- Griffin, O.M. 1995 A note on bluff body vortex formation. *J. Fluid. Mech.* **284**, 217-224.
- Grue, J., Jensen, A., Rusas, P., and Sveen, J.K. 2000 Breaking and broadening of internal solitary waves. *J. Fluid Mech.* **413**, 181-217.
- Karasso, P. S. and Mungal, M. G. 1997 PLIF measurements in aqueous flows using the Nd:Yag laser. *Exp. Fluids* **23**, 382-387.

Konstantinidis, E., Balabani, S., and Yianneskis, M. 2003 The effect of flow perturbations on the near wake characteristics of a circular cylinder. *J. Fluids and Structures* **18**, 367-386.

Kukulka, D.J. 1981 Thermodynamics and transport properties of pure and saline water. M.S. thesis, State University of New York at Buffalo.

Lawrence, G.A. and Browand, F.K. 1991 The stability of a sheared density interface. *Phys. Fluids A* **3**(10), 2360-2370.

Lin, J-T and Pao, Y-H. 1979 Wakes in stratified fluids. *Ann. Rev. Fluid Mech.* **11**, 317-338.

Lindl, J. D., 1998 *Inertial Confinement Fusion: The Quest for Ignition and Energy Gain Using Indirect Drive*, Springer-Verlag.

Ng, K.H. and Spalding, D.B. 1972 Turbulence model for boundary layers near walls. *Phys. Fluids* **15**(1), 20-30.

Norberg, C. 1986 Interaction of free stream turbulence and vortex stretching for a single tube in cross-flow. *J. Wind Eng. and Industrial Aero.* **23**, 501-514.

Oosthuizen, P.H. and Madan, S. 1971 The effect of flow direction on combined convective heat transfer from cylinders to air. *J. Heat Transfer* **93**, 240-242.

Pao, Y. 1973 Measurements of internal waves and turbulence in two-dimensional stratified shear flows. *Boundary-Layer Meteorology* **5**, 177-193

Ramaprabhu, P. 2003 On the Dynamics of Rayleigh-Taylor Mixing. Ph.D. dissertation, Texas A&M University.

Ramaprabhu, P. and Andrews, M.J. 2004 Experimental investigation of Rayleigh-Taylor mixing at small atwood numbers. *J. Fluid Mechanics* **502**, 233-271.

- Read, K.I. 1984 Experimental investigation of turbulent mixing by Rayleigh-Taylor instability. *Physica D* **12**, 45-58.
- Rodi, W. 1993 *Turbulence Models and Their Application in Hydraulics, A State-of-the-Art Review*. A.A. Balkema.
- Snider, D.M. and Andrews, M.J. 1994 Rayleigh-Taylor and shear driven mixing with an unstable stratification. *Phys. Fluids* **6**(10), 3324-3334.
- Snider, D.M. and Andrews, M.J. 1996 The simulation of mixing layers driven by compound buoyancy and shear. *ASME J. Fluids Engineering* **118**(2), 370-376.
- Spedding, G.R. 1997 The evolution of initially turbulent bluff-body wakes at high internal Froude number. *J. Fluid. Mech.* **337**, 283-301
- Spedding G.R. 2002 Vertical structure in stratified wakes with high initial Froude number. *J. Fluid. Mech.* **454**, 71-112.
- Turner, J.S. 1973 *Buoyancy Effects in Fluids*. Cambridge University Press.
- Unal, M.F. and Rockwell, D. 1988 On vortex formation from a cylinder. Part1. The initial instability. *J. Fluid Mech.* **190**, 491-512.
- Waddell, J.T., Nedierhaus, C.E. and Jacobs, J.W. 2001 Experimental study of Rayleigh-Taylor instability: Low Atwood number liquid systems with single-mode initial perturbations. *Phys. Fluids* **13**, 1263-1273.
- Walker, D.A. 1987 A fluorescence technique for measurement of concentration in mixing liquids. *J. Phys. E: Sci. Instrum.* **20**, 217-224
- Williamson, C.H.K. 1996 Vortex dynamics in the cylinder wake. *Annu. Rev. Fluid. Mech.* **28**, 477-534.

Wilson, P.N. 2003 A study of buoyancy and shear driven turbulence within a closed water channel. Ph.D. dissertation, Texas A&M University.

Wilson, P.N. and Andrews, M.J. 2002 Spectral measurements of Rayleigh-Taylor mixing at small Atwood number. *Phys. Fluids* **14**(3), 938-945.

Xu, Y., Fernando, J.S., and Boyer D.L. 1995 Turbulent wakes of stratified flow past a cylinder. *Phys. Fluids* **7**(9), 2243-2255.

Youngs, D.L. 1984 Numerical simulation of turbulent mixing by Rayleigh-Taylor instability. *Physica D* **12**, 32-44.

Youngs, D.L. 1990 Three-dimensional numerical simulation of turbulent mixing by Rayleigh-Taylor instability. *Phys. Fluids A* **3**(5), 1312-1320.

## APPENDIX A

### SYCHRONIZATION OF THE DIGITAL CAMERA AND LASER SYSTEM

During the course of the current research, the previous method of synchronization of the digital camera and lasers required replacement. The method chosen for future triggering and synchronization of the camera and lasers is the use of a programmable pulse generator. The pulse generator chosen is Model 555-2C from Berkley Nucleonics, Inc.. The selected model allows input of an external trigger signal which can be manipulated through a user interface to output up to two signals. A TTL triggering pulse of 30 Hz output by the digital camera is divided by the pulse generator into two 15 Hz signals 180° out of phase with respect to each other. These two 15 Hz signals are then used to trigger the flash lamp of the respective lasers. Attention should be paid to the operating procedure and system settings for the pulse generator contained on the subsequent pages.

*A.1 Model 555-2C Pulse Generator Setup for Laser / Camera Synchronization*

General Settings:                    Mode :            Single Mode  
    Gate/Trig:        Extin – Triggered  
    Level – 2.50  
    Edge – Falling

Channel A:                            Width: 1 micro sec  
    Delay: 0  
    Pol: Active High  
    Out: TTL/CMOS  
    Mode: Divide-By-N  
    /n: 2  
    Gate: Disabled

Channel B:                            Width: 1 micro sec  
    Delay: 0.068799449 sec  
    Pol: Active High  
    Out: TTL/CMOS  
    Mode: Normal  
    Gate: Disabled

Notes:

Channel A triggers from the external trigger output from the camera. The divide by n mode with  $n = 2$  results in a 15 Hz output signal.

Channel B triggers from Channel A with this setup, not the external trigger signal from the camera. Therefore the operation is set to Normal instead of divide by n. A delay is used to adjust the output to 180 degrees out of phase of Channel A.

All settings are saved under: Recall #: 1 , User: Lasers

### *A.2 Operating Procedure for Model 555-2C Pulse Generaor*

1. Disconnect output and external trigger cables.
2. Turn on the pulse generator.
3. Reconnect output and external trigger cables.
4. Press "Function" then "Recall"
5. Use next button to find Recall #: 1 , User: Lasers.
6. Press "Function" then "Recall" to load the settings.
7. With camera on and connected to PIV capture computer, open Labview on capture computer. ( 11Jan2000 Shortcut ). Press “Run” button on Labview interface, which inverts the TTL signal initially output by the camera when power is turned on.

(This step is necessary for the triggering system to operate properly.)

8. When ready to externally trigger lasers, return to the pulse generator and press "Run".
9. When finished with the laser system, press “Run” to stop the pulse generator.



**APPENDIX B**

**SOLUTIONS FOR THE MATHEMATICAL MODEL OF VELOCITY**

**FLUCTUATIONS IN THE NEAR WAKE**

The general form of the model for the decay of vertical velocity fluctuations in the near wake including the effects of buoyancy is

$$\frac{dv'}{dt} = av'^2 + bv + c$$

where

$$a = -\frac{3^{1/2}}{2^{3/2}} \frac{C_D}{D}$$

$$b = 0$$

$$c = -\left(\frac{1}{6}\right)^{1/2} \frac{\Delta\rho}{\rho} g$$

Analytical solutions for an equation of this type, which can be written in the following form

$$\int \frac{dv'}{av'^2 + bv' + c}$$

are dependent on the sign of  $(b^2 - 4ac)$ . The values of  $(b^2 - 4ac)$  for the wake with no buoyancy, stable buoyancy, and unstable buoyancy are shown below.

No buoyancy:  $(b^2 - 4ac) = (0)^2 - 4(0) = 0$

Stable buoyancy:  $(b^2 - 4ac) = (0)^2 - 4(-)(-) < 0$

Unstable buoyancy:  $(b^2 - 4ac) = (0)^2 - 4(-)(+) > 0$

### B.1 No buoyancy solution

When  $(b^2 - 4ac)$  is equal to zero the analytical solution is of the form

$$\int \frac{dv'}{av'^2 + bv' + c} = \frac{-2}{2av' + b}.$$

Applying this solution to the wake with no buoyancy yields the following general solution

$$v' = \frac{1}{-at + C_1}.$$

The integration constant,  $C_1$ , is solved for by treating the peak value of the  $v'_{rms}$  as an initial condition, where  $v' ( t=0 ) = v'_{peak}$ . The final solution for the wake without buoyancy, using this initial condition is

$$v' = \frac{1}{\left( -at + \frac{1}{v'_{peak}} \right)}.$$

### B.2 Stable buoyancy solution

The solution for the stable buoyancy solution is found in a similar manner.

When  $(b^2 - 4ac) < 0$ , the analytical solution is of the form

$$\int \frac{dv'}{av'^2 + bv' + c} = \frac{2}{(4ac - b^2)^{1/2}} \arctan \left( \frac{2av' + b}{(4ac - b^2)^{1/2}} \right).$$

Simplifying this expression, the solution for the wake with stable buoyancy is

$$\frac{1}{(ac)^{1/2}} \arctan \left( \frac{av'}{(ac)^{1/2}} \right) = t + C_1.$$

Solving for  $v'$

$$v' = \frac{(ac)^{1/2}}{a} \tan((ac)^{1/2}t + C_2)$$

Again treating the peak value of the  $v'_{rms}$  as an initial condition the stable buoyancy solution becomes

$$v' = \frac{(ac)^{1/2}}{a} \tan\left((ac)^{1/2}t + \arctan\left(\frac{a v'_{peak}}{(ac)^{1/2}}\right)\right)$$

### B.3 Unstable buoyancy solution

For the wake with unstable buoyancy the value of  $(b^2 - 4ac) > 0$  resulting in a solution which has the general form of

$$\int \frac{dv'}{av'^2 + bv' + c} = \frac{1}{(b^2 - 4ac)^{1/2}} \ln\left(\frac{2av' + b - (b^2 - 4ac)^{1/2}}{2av' + b + (b^2 - 4ac)^{1/2}}\right)$$

Simplifying this solution for the wake with unstable buoyancy,

$$\frac{1}{(-4ac)^{1/2}} \ln\left(\frac{2av' - (-4ac)^{1/2}}{2av' + (-4ac)^{1/2}}\right) = t + C_1$$

To further simplify the solution the following identity is used

$$\arctan h(\chi) = \frac{1}{2} \ln\left(\frac{1+\chi}{1-\chi}\right) \text{ when } \chi^2 < 1.$$

Rewriting the solution into a similar form,

$$\frac{1}{2} \ln\left(\frac{1 - \left(\frac{-c}{av'^2}\right)^{1/2}}{1 + \left(\frac{-c}{av'^2}\right)^{1/2}}\right) = (-ac)^{1/2}t + C_2$$

Letting  $d = \left( \frac{-c}{av'^2} \right)$

$$\frac{1}{2} \ln \left( \frac{1-d^{1/2}}{1+d^{1/2}} \right) = (-ac)^{1/2} t + C_2$$

The square root of  $d$  can be chosen to be (+) or (-) depending on the desired behavior of the solution. For a decaying solution the square root of  $d$  is chosen to be (-).

$$\frac{1}{2} \ln \left( \frac{1-(-1)d^{1/2}}{1+(-1)d^{1/2}} \right) = (-ac)^{1/2} t + C_2$$

The identity for the hyperbolic function can then be applied where  $\chi = d^{1/2} = \left( \frac{-c}{av'^2} \right)^{1/2}$ ,

yielding

$$\operatorname{arctanh}(d^{1/2}) = (-ac)^{1/2} t + C_3$$

This expression is now solved for  $v'$ .

$$v' = \frac{\left( \frac{-c}{a} \right)^{1/2}}{\tanh \left( (-ac)^{1/2} t + C_3 \right)}$$

The integration constant,  $C_3$ , is obtained by treating the peak value of the  $v'_{rms}$  as an initial condition, where  $v'(t=0) = v'_{peak}$ . The final solution for the wake with unstable buoyancy, using this initial condition is

$$v' = \frac{\left(\frac{-c}{a}\right)^{1/2}}{\tanh\left((-ac)^{1/2}t + \operatorname{arctanh}\left(\frac{\left(\frac{-c}{a}\right)^{1/2}}{v'_{peak}}\right)\right)}.$$

**VITA**

Name: Wayne N. Kraft

Date and place of birth: April 22, 1979  
Wilmington, Delaware  
USA

Permanent Address: 2065 River Oaks Dr.  
New Braunfels, Texas 78132

Education: B.S. (Mechanical Engineering), December 2001  
Texas A&M University, College Station, Texas

M.S. (Mechanical Engineering), August 2004  
Texas A&M University, College Station, Texas